Research article

JHEP|Reports

Albumin reprograms the B cell transcriptional landscape and improves neutrophil antimicrobial function in patients with decompensated cirrhosis

Joan Clària[1,2,3,4,*,†], **Ferran Aguilar**[1,†], **Juan-José Lozano**[3,†], **Laura Jiménez-Gracia**[4,5,†], **Juan C. Nieto**[4,5,†], Berta Romero-Grimaldo[1,2,3], Xavi Marcos-Fa[6], Emma Giarracco[6], Emmanuel Weiss[1,7,8], Jonel Trebicka[1,9], Inmaculada Hernàndez[4,5,10], Javier Fernandez[1,2], Mireia Casulleras[1,2], Cristina López-Vicario[1,2,3], Sinan Muldur[11], Alex Hopke[11], Alexandru Vlagea[2], Ana M. Aransay[3,12], Domenica Marchese[4,5], Mauro Bernardi[13], Rajiv Jalan[1,14], Paolo Angeli[1,15], Giuliana Magri[16], Andrea Cerutti[6,17], Daniel Irimia[11], Holger Heyn[4,5,‡], Vicente Arroyo[1,‡], Richard Moreau[1,7,18,*,‡]

JHEP Reports **2024**. vol. 6 | 1–15

Check for updates

Background & Aims: Patients with acutely decompensated (AD) cirrhosis are immunocompromised and particularly susceptible to infections. This study investigated the immunomodulatory actions of albumin by which this protein may lower the incidence of infections.

Methods: Blood immunophenotyping was performed in 11 patients with AD cirrhosis and 10 healthy volunteers (HV). Bulk and single-cell RNA sequencing (scRNA-seq) and flow cytometry were performed in peripheral blood mononuclear cells (PBMCs) from 20 patients with AD cirrhosis and 34 HV exposed to albumin. Albumin's effects on degranulation, phagocytosis, chemotaxis, and swarming of neutrophils from six patients with AD cirrhosis and nine HV were assessed by measuring myeloperoxidase enzymatic activity, the engulfment of fluorescent-labeled *Escherichia coli* and zymosan, and interactions of neutrophils with *Candida albicans* at single-cell resolution in microfluidic chambers, respectively. Whole blood RNA sequencing (RNA-seq) analyses were performed in 49 patients admitted for severe AD cirrhosis, of whom 30 received albumin during hospitalization.

Results: Compared with HV, patients with AD cirrhosis showed severe lymphopenia and defective neutrophil antimicrobial function. Bulk and scRNA-seq analyses revealed significantly (false discovery rate [FDR] <0.05) increased signatures related to B cells, myeloid cells, and $CD4^+$ T cells in PBMCs incubated with albumin. Changes in the B cell population were confirmed by flow cytometry. Neutrophils exposed to albumin also exhibited augmented chemotactic and degranulation responses, enhanced phagocytosis, and increased pathogen-restrictive swarming. RNA-seq data analysis in patients who had received albumin revealed specific upregulation of signatures related to B cells and neutrophils together with transcriptional changes in $CD4^+$ T cells (FDR <0.05).

Conclusions: The finding that albumin promotes the transcriptional reprogramming and expansion of the B cell compartment and improves neutrophil antimicrobial functions indicates mechanisms that may lower the incidence of infections in patients with severe AD cirrhosis receiving albumin therapy.

© 2024 The Author(s). Published by Elsevier B.V. on behalf of European Association for the Study of the Liver (EASL). This is an open access article under the CC BY-NC-ND license (http://creativecommons.org/licenses/by-nc-nd/4.0/).

Introduction

Acute decompensation is the most frequent cause of nonelective hospital admission of patients with cirrhosis, and its most severe form, acute-on-chronic liver failure (ACLF), is characterized by hepatic and/or extrahepatic organ failures and high risk of short-term death.[1,2] These patients exhibit intense systemic inflammation, indicated by leukocytosis,[2,3] elevated blood levels of cytokines, inflammatory lipid mediators, and C-reactive protein (CRP).[1,3–5] These patients also exhibit immunosuppression, indicated by decreased responses of specific monocyte subsets to bacterial products,[6,7] decreased capacity to kill microbes,[6,8,9] and reduced lymphocyte function.[3] Immunosuppression predisposes patients with acutely decompensated (AD) cirrhosis to secondary infections and re-escalation of end-organ dysfunction and mortality.[10] To date, there are no therapies to prevent or treat patients with AD cirrhosis who are immunocompromised or have an impaired immune response. This unmet need is more striking given the ramping prevalence of patients with AD cirrhosis infected with Gram-positive or Gram-negative bacteria resistant to antibiotics.[11]

Albumin therapy is common in patients with AD cirrhosis, including patients treated with large-volume paracentesis and

* Corresponding authors. Address: EF CLIF, Travessera de Gràcia 11, 7th Floor, 08021, Barcelona, Spain.
E-mail addresses: richard.moreau@inserm.fr (R. Moreau), jclaria@clinic.cat (J. Clària).
† Co-first authors.
‡ Co-senior authors.
https://doi.org/10.1016/j.jhepr.2024.101184

patients with spontaneous bacterial peritonitis (SBP) or hepatorenal syndrome–acute kidney injury (HRS-AKI).[12] Recently, the ANSWER study has demonstrated a lower incidence of SBP and other infections in patients with AD cirrhosis receiving long-term weekly administration of albumin.[13] In addition, albumin administration has emerged as an efficacious anti-inflammatory therapy, reducing cytokine levels in patients with AD cirrhosis and ACLF.[14] Although albumin pleiotropic effects have classically been attributed to its oncotic and antioxidant properties,[15] recent data on leukocytes from patients with AD cirrhosis have shown that albumin modulates cytokine production in response to bacterial DNA by interacting with the endosomal TLR9 signaling pathway.[16] The albumin immune restorative effects have also been linked to inactivation of the immunosuppressive effects of PGE_2.[8] However, at present, a comprehensive and deep understanding of the immunomodulatory actions of albumin in the setting of AD cirrhosis is still lacking.

To assess this, we designed *in vitro* experiments and performed bulk and single-cell RNA-sequencing (scRNA-seq) and functional assays in peripheral blood mononuclear cells (PBMCs) and neutrophils from patients with AD cirrhosis and healthy volunteers (HV). Confirmatory *in vivo* whole blood RNA sequencing (RNA-seq) studies were performed in 30 patients with severe AD cirrhosis receiving albumin therapy and in 19 non-albumin-treated patients with AD cirrhosis from the PREDICT study.[17] The results of this investigation revealed that albumin induces specific immune cell gene signatures primarily related to the revitalization of B cell and neutrophil defensive functions in patients with AD cirrhosis. These findings expand our understanding of the mechanisms whereby albumin lowers the rate of infections in patients with cirrhosis and improves survival.

Patients and methods

Patients

For immunophenotyping and *in vitro* experiments in PBMCs, peripheral blood was obtained from 20 patients with AD cirrhosis recruited at the Liver Intensive Care Unit of the Hospital Clínic of Barcelona and 34 HV from the Barcelona Hospital Clínic Blood Bank (Table S1). For neutrophil experiments, peripheral blood was obtained from six patients with AD cirrhosis and nine age-matched HV (Table S2). Whole blood bulk RNA-seq was performed in 10 HV and 49 patients with AD cirrhosis from the PREDICT study,[17] of whom 30 had received albumin therapy (see Supplementary methods for selection criteria). All patients provided written informed consent to participate, and approval was granted by the Ethics Committee of the Hospital Clínic of Barcelona (#HCB/2016/0710, #HCB/2018/0899 and #HCB/2015/0427).

Immunophenotyping and isolation of PBMCs and neutrophils

See Supplementary methods.

PBMC incubations

PBMCs (1.5–3.0 × 10^6 cells/ml) seeded in RPMI 1640 medium were incubated with either human serum albumin (HSA, Albutein®, Grifols, Barcelona, Spain), recombinant albumin expressed in *Oryza sativa* (Sigma-Aldrich, St Louis, MO, USA) (both at 15 mg/ml), or a vehicle control for 24 h at 37 °C in a 5% CO_2 incubator. For comparison, experiments with the isooncotic compound mannitol (Sigma-Aldrich) (15 mg/ml), albumin-depleted FBS (15% total volume), and IgG from human serum (Sigma-Aldrich) (15 mg/ml) were also performed. Albumin-depleted FBS was prepared using the Pierce™ Albumin Depletion Kit, and depletion was verified using the bicinchoninic acid assay. In some experiments, PBMCs were incubated with the neonatal Fc receptor (FcRn) blocking antibody ADM31 (Aldevron, Fargo, ND, USA) (10 μg/ml) before the addition of albumin.

Bulk RNA-seq in whole blood

Isolation of total RNA from whole blood collected in Tempus tubes, assessment of RNA concentration and integrity, library preparation, sequencing, and processing of RNA-seq data are described in the Supplementary methods.

Bulk RNA-seq and real-time PCR in PBMCs

See Supplementary methods.

scRNA-seq in PBMCs

PBMCs (1.5 × 10^6 cells/ml) seeded in RPMI 1640 medium were incubated with either HSA (15 mg/ml) or the vehicle (culture medium) for 2 h at 37 °C in a 5% CO_2 incubator. At the end of the incubation period, cells were rapidly (within 30 min) transferred on ice to the CNAG Single Cell Genomics platform (see Supplementary methods).

Neutrophil degranulation and phagocytosis assays

See Supplementary methods.

Neutrophil chemotaxis and swarming assays

A chemotaxis–phagocytosis assay in microfluidic arenas[18] was used to test the role of HSA on the ability of neutrophils to migrate directionally toward and to phagocytose *Candida albicans* yeast. A swarming assay was used to test the contribution of HSA to the ability of neutrophils to contain the growth of *Candida* clusters. To this purpose, arrays of *Candida*-adherent spots (200-μm diameter) were printed using a microarray printing platform (Picospotter PolyPico, Galway, Ireland) and a solution of poly-l-lysine (Sigma-Aldrich) (see Supplementary methods).

Results

Characterization of the blood immune cell landscape in patients with AD cirrhosis

The peripheral immune cell landscape was characterized by flow cytometry in a representative population of patients with AD cirrhosis in whom HSA administration was indicated as standard of care. Compared with HV, patients with AD cirrhosis showed neutrophilia, severe lymphopenia, and monocytosis (Fig. 1A). Lymphopenia affected $CD8^+$ lymphocytes and natural killer (NK) cells (Fig. 1B). The analysis of $CD45^+CD19^+$ B lymphocytes, which included the study of distinct B cell subsets defined using specific gating strategies (Fig. 1C), also revealed a decline of B and transitional B cells in patients with AD cirrhosis, suggesting impaired B-cell development and maturation (Fig. 1D).

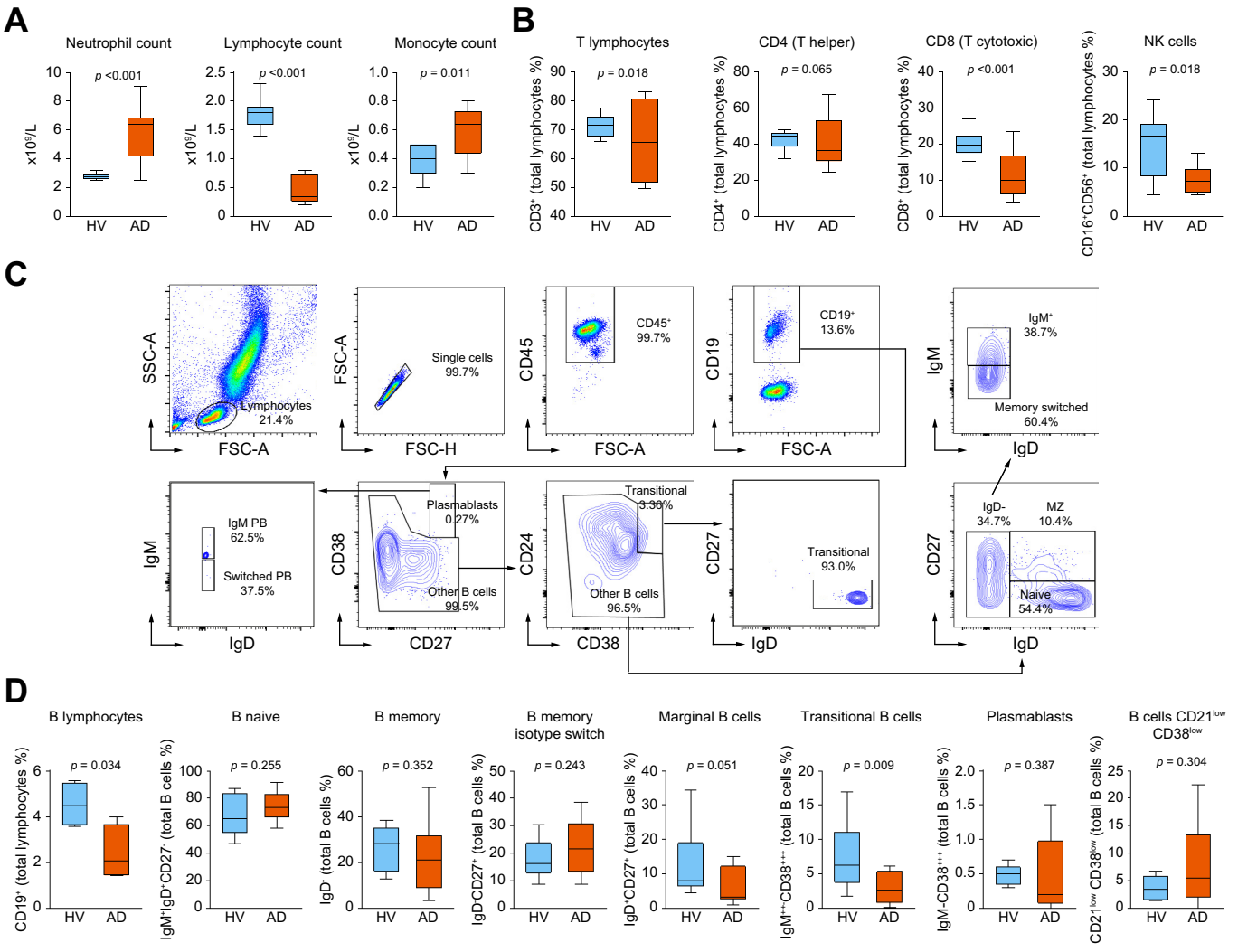

Fig. 1. Peripheral immune cell landscape of patients with AD cirrhosis. (A) Peripheral blood cell counts in 10 HV and 11 patients with AD cirrhosis. (B) Peripheral blood immunophenotyping of T cells, $CD4^+$ and $CD8^+$ T cells, and NK cells in HV and patients with AD cirrhosis. (C) Scatterplots of the flow cytometry analysis showing the gating strategy to identify the different B cell subtypes, including plasmablasts ($CD45^+CD19^+CD38^{++}CD27^{++}$), transitional ($CD45^+CD19^+CD38^{++}CD24^+IgD^+CD27^-$), naïve ($CD45^+CD19^+IgD^+CD27^-CD24^{low}IgM^+$), marginal ($CD45^+CD19^+IgD^+CD27^+CD24^{high}IgM^{++}$), and switched ($CD45^+CD19^+IgD^-CD27^{+/-}IgM^-$). (D) Proportions of B cells and subpopulations in the peripheral blood of HV and patients with AD cirrhosis. Box and whisker graphs in panels A, B, and D represent the median (IQR). Lower and upper box borders indicate the 25th and 75th percentiles, respectively. Lines within each box indicate median percentage. Whiskers above and below each box indicate maximum and minimum values, respectively. Significance between groups was obtained using Wilcoxon–Mann–Whitney tests. AD, acutely decompensated; HV, healthy volunteers; NK, natural killer.

In vitro response of mononuclear leukocytes from patients with AD cirrhosis to HSA

To investigate the direct effect of HSA on immune cells avoiding any confounding factor present in the patient's bloodstream, we first performed experiments *in vitro* in PBMCs isolated from patients with AD cirrhosis. To accurately assess the global transcriptional changes elicited by albumin, we performed bulk RNA-seq and identified differentially expressed (DE) gene sets by gene set enrichment analysis (GSEA). This analysis identified two clusters of gene sets related to B-cell-mediated immunity, B-cell activation, immunoglobulin complexes, immunoglobulin receptor binding, immunoglobulin production, immune response mediated by immunoglobulins, and the B cell receptor signaling pathway that were significantly enriched in PBMCs incubated with HSA (Fig. 2A). Among the gene clusters enriched by HSA, we also identified three gene sets related to the Fc receptor signaling pathway (Fig. 2A). HSA also induced the enrichment of two additional gene set clusters, one related to T cells and DNA and protein complexes and the other to antimicrobial responses, phagocytosis recognition, and defense response against bacteria (Fig. 2A). To exclude the possibility that the effect of HSA on PBMCs could be caused by the presence of stimulatory serum factors bound to its molecule and retained during its manufacturing, we repeated the experiments using recombinant human albumin from *Oryza sativa*. These experiments confirmed that the activation of the B

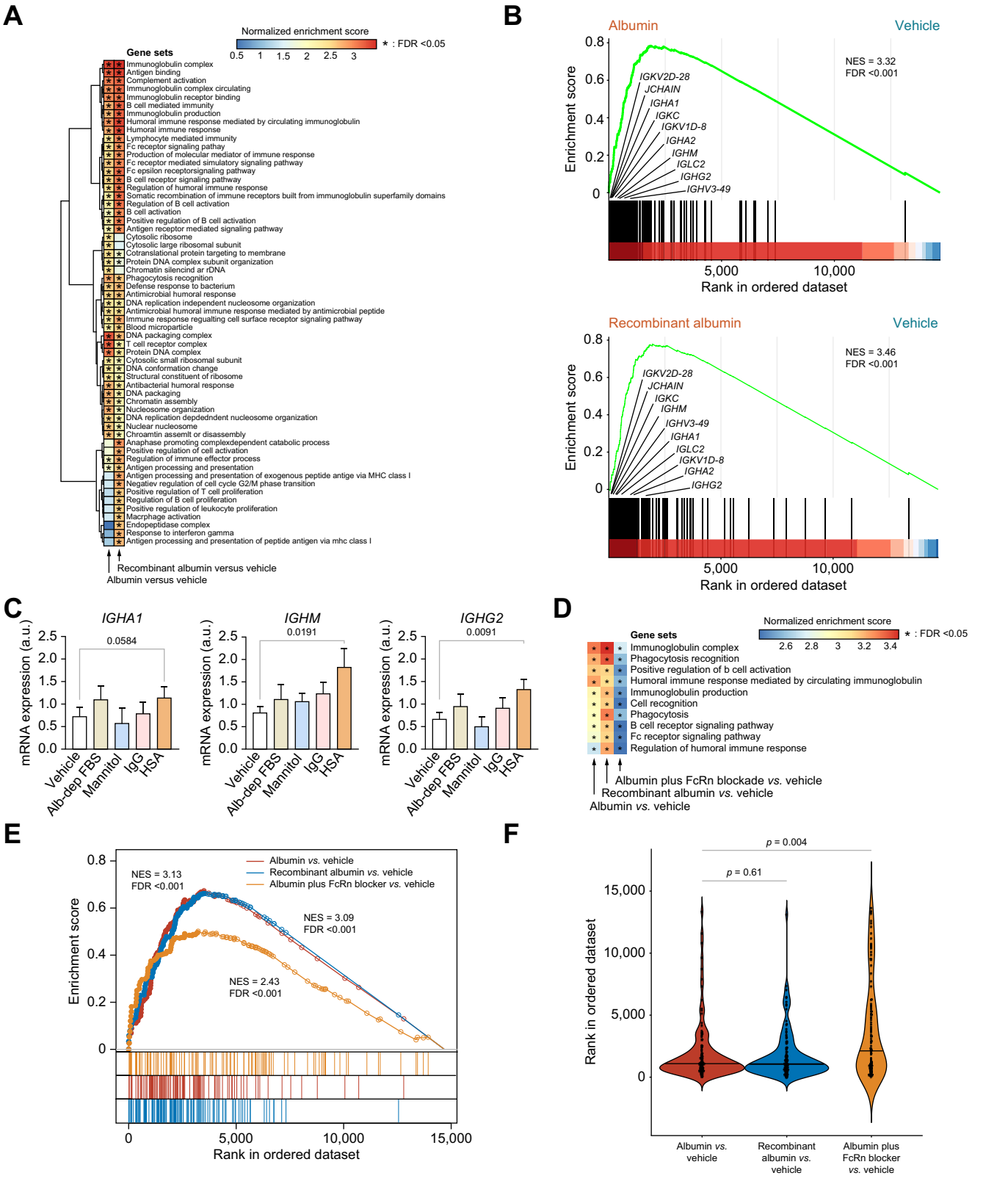

Fig. 2. Changes in the transcriptional landscape of PBMCs isolated from patients with AD cirrhosis and incubated *in vitro* with HSA. (A) GSEA was run on RNA-seq data to generate ranked lists of genes for the two following pairwise comparisons *vs*. vehicle: HSA and recombinant albumin (both at 15 mg/ml). Color gradient corresponds to increasing values of the NES of gene sets from the less (in blue) to the most (in red) upregulated. Asterisks in the heat map indicate FDR <0.05. (B) GSEA enrichment plots of the immunoglobulin complex gene set in two comparisons *vs*. vehicle: HSA (top) and recombinant albumin (bottom). The hash plot under GSEA curves shows where the members of the gene set appear in the ranked list of genes. The genes shown on the plots are representative of leading-edge genes (*i.e.* top-scoring genes). (C) Changes in the expression of three representative leading-edge genes coding for immunoglobulins in response to the vehicle control, 15% albumin-

cell transcriptome by albumin is an intrinsic property of this molecule (Fig. 2A). Similar results were observed in PBMCs isolated from HV, indicating that the effect of albumin on B cells was not exclusive to patients with cirrhosis (Fig. S1). Moreover, enrichment analysis identified several leading-edge genes coding for immunoglobulins increased by both HSA and recombinant albumin (Fig. 2B). To assess whether the effect of HSA on immunoglobulin expression was related to its oncotic properties, we compared the effects of HSA with those of the iso-oncotic control mannitol, IgG, and albumin-depleted FBS and demonstrated that leading-edge immunoglobulin genes were only upregulated by HSA (Fig. 2C).

FcRn is implicated in the B cell response to HSA

Having shown that albumin enhances the expression of gene sets related to the Fc receptor signaling pathway, we explored whether the B cell stimulatory effect of HSA was mediated by its binding to FcRn, an Fc receptor that binds albumin with high affinity.[19] The normalized enrichment score (NES) for the immunoglobulin complex in PBMCs incubated with HSA in the presence of an FcRn-blocking antibody was lower than that in PBMCs incubated with HSA alone (Fig. 2D and E). Consistent with this, immunoglobulin genes showed a less preferred position in the ordered ranked list of genes in PBMCs incubated with HSA in the presence of the FcRn blocker than in PBMCs incubated with HSA alone (Fig. 2F). Although these findings suggest some implication of the FcRn receptor in the transcriptional reconfiguration of B cells elicited by HSA, other receptors or mechanisms are also likely involved in this transcriptional rearrangement.

Profile of the *in vitro* effects of HSA at the scRNA-seq level

We next used scRNA-seq to gain a deeper insight into the multitiered complexity of the cellular composition of PBMCs exposed *in vitro* to HSA for 2 h. We jointly analyzed 66,064 human PBMCs from nine patients with AD cirrhosis clustered into B lymphocytes, T lymphocytes, and myeloid cells. Each lineage was subclustered to define fine-grained cell populations using canonical gene markers (Figs. S2 and S3). We then analyzed 1,946 B lymphocytes and identified 10 principal populations, including two subpopulations that acquired a transitional-like B cell profile characterized by a higher expression of *CD79B*, *IGHD*, and *TCL1A* (transitional 1 B cell) along with a higher expression of *CD55* (transitional 2 B cell) (Fig. 3A). HSA increased the frequency of B cells expressing a transitional-like profile while reducing naive B cells (Fig. 3B and C). To further confirm that HSA induced transcriptional changes resembling those of transitional-like B cells, we assessed the expression of specific genes described by Steward *et al.*[20] This analysis proved the HSA-induced expression of *TCL1A*, *VPREB3*, *PCDH9*, *IGHM*, and *IGHD* genes in transitional B cells (Fig. S4). Importantly, HSA-induced increased frequency of transitional-like B cells observed at the transcriptional level was confirmed by flow cytometry at 24 h (Fig. 3D and E). Interestingly and consistent with the essential role of albumin in *in vitro* B-cell growth,[21] a significant increase in the B cell population was detected by flow cytometry (Fig. 3E). However, albumin did not expand any other B cell subset (Fig. S5A). In addition, no effects on B cells were observed in response to albumin-depleted FBS, mannitol, or IgG (Fig. S5B).

In addition to B cells, we also assessed 21,677 myeloid cells, which clustered into 13 different cell populations of monocytes (n = 7), dendritic cells (n = 3), and myeloid-derived suppressor cells and granulocyte-monocyte progenitors (n = 3) (Fig. 3F). Fig. 3G and H shows that HSA increased the frequency of monocytes with an HAVCR2$^+$ intermediate transcriptional signature and plasmacytoid dendritic cells. The HSA-induced shift in the HAVCR2$^+$ intermediate monocyte population was unlikely attributed to the upregulation of surface proteins resulting from cell attachment, as no changes were observed in the expression of genes associated with monocyte activation (*i.e. FCGR3A*, *CD80*, *CD86*, *ICAM1*, *ITGAM*, *CCR2*, and *HLA*)[22] (Fig. S6A). HSA did not change the frequency of other myeloid cell populations (Fig. S6B).

We also analyzed 17,467 T lymphocytes, including 12,692 CD4$^+$ T cells, 3,483 CD8$^+$ T cells, and 1,292 unconventional T cells. Interestingly, HSA modified the frequency distribution of the 10 populations captured within the CD4$^+$ T cell compartment (Fig. 3I–K and Fig. S7). Specifically, HSA decreased the frequency of activated memory CD4$^+$ T cells while increasing central memory ITGB1$^+$ CD4$^+$ T cells (Fig. 3K). Finally, no significant changes were found upon HSA exposure within the 13 populations of CD8$^+$ T cells and unconventional T cells (Fig. S8). Together, these observations confirmed at the single-cell level the ability of HSA to reprogram the transcriptional landscape of B cells and other mononuclear leukocytes isolated from patients with AD cirrhosis.

In vitro response of polymorphonuclear leukocytes (neutrophils) from patients with AD cirrhosis to HSA

To have a more comprehensive view of the effects of HSA on blood immune cells, we designed *in vitro* experiments in neutrophils from patients with AD cirrhosis and HV. Given that neutrophils express fewer genes than any other leukocyte and that their lower RNA content complicates high-throughput transcriptomic analysis,[23] we tested the effects of HSA on neutrophil function, including degranulation, phagocytosis, chemotaxis, and swarming. As expected, neutrophils from

depleted FBS (Alb-dep FBS), mannitol (15 mg/ml), IgG (15 mg/ml), and HSA (15 mg/ml). Significant differences between groups were assessed using *t* tests. (D) Heat map of the NES for the 10 representative B cell–related gene sets obtained for each of the following three comparisons *vs.* vehicle: HSA, recombinant albumin, and FcRn blocker (10 μg/ml) plus HSA *vs.* vehicle. (E) Enrichment plots of the immunoglobulin complex in the three GSEA comparisons described in D. The leading-edge genes are indicated by solid dots. The hash plots under GSEA curves show where the members of the gene set appear in each of the three ranked lists of genes. (F) Rank order of each gene of the immunoglobulin complex gene set. The higher in the rank, the lower the importance. Values of *p* are ranked from Kruskal–Wallis tests, followed by Mann–Whitney *U* tests. All FDR values are computed with adjustments for multiple testing and gene set size in the GSEA analysis. AD, acutely decompensated; FcRn, neonatal Fc receptor; FDR, false discovery rate; GSEA, gene set enrichment analysis; HSA, human serum albumin; HV, healthy volunteers; NES, normalized enrichment score; PBMC, peripheral blood mononuclear cell; RNA-seq, RNA sequencing.

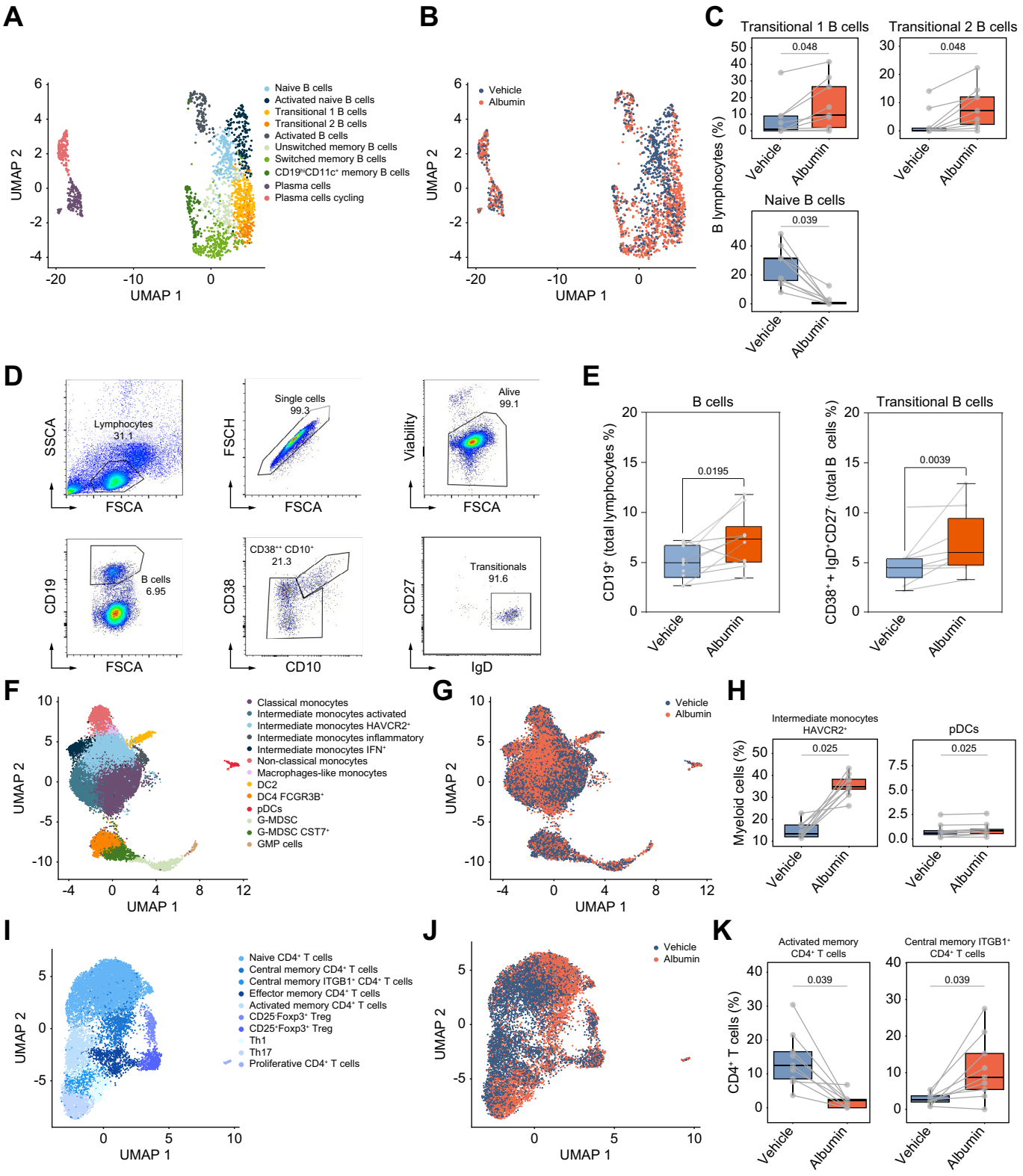

Fig. 3. scRNA-seq and flow cytometry analyses identify specific immune cell changes in PBMCs exposed *in vitro* to HSA. (A) UMAP of 1,946 patients' B cells exposed to HSA and the vehicle, colored by cell types. (B) Overlay of HSA and vehicle exposure on the B lymphocyte UMAP. (C) Box plots for the proportion of B cell populations that significantly changed after HSA exposure. (D, E) Scatterplots of the flow cytometry analysis showing the gating strategy to identify B and transitional B cells and boxplots showing their proportions after HSA exposure. (F) UMAP of 21,819 patients' myeloid cells exposed to HSA and the vehicle, colored by cell populations. (G) Overlay of HSA and vehicle exposure on the myeloid cell UMAP. (H) Box plots for the proportion of myeloid cell types that significantly changed after

patients with AD cirrhosis showed impaired antimicrobial functions, including impaired phagocytosis, which is consistent with previous studies,[9] as well as reduced neutrophil chemotaxis and swarming (Fig. S9). Incubation of neutrophils from both patients with AD cirrhosis and HV with either HSA or recombinant human albumin increased degranulation, as assessed by myeloperoxidase (MPO) activity in the supernatant (Fig. 4A), an essential antimicrobial protein localized mainly to the azurophil or primary neutrophil granules.[24] Incubation of neutrophils from both patients with AD cirrhosis and HV with either HSA or recombinant human albumin also increased phagocytosis, as monitored by the ingestion of fluorescent-labeled zymosan particles by neutrophils (Fig. 4B). The phagocytosis findings were confirmed using fluorescent-labeled *Escherichia coli* (Fig. S10). We finally tested the effect of HSA on neutrophil swarming, a defensive process in which neutrophils undergo phases of highly directed and coordinated migration, followed by accumulation at sites of infection that culminate in the containment and killing of the intruding pathogen. Here, we used microfluidic devices that enable monitoring at single-cell resolution the neutrophil interactions with *Candida* through morphology changes from yeast to hyphae and hyphae growth.[18] We also tested the effect of HSA on neutrophil phagocytosis of live *Candida*. Neutrophils from patients displayed severe defects in their ability to control fungal growth, as measured by the time it took for *Candida* hyphae to escape the neutrophil swarm and the higher total area covered by fungal growth (Fig. S9). The addition of HSA improved the ability of neutrophils to restrict fungal growth in a concentration-dependent manner (higher albumin leading to greater restriction) (Fig. 4C). Imaging showed that in the presence of HSA, neutrophils swarmed around any *Candida* hyphae clusters, phagocytosing them and delaying their growth (Fig. 4D and Supplementary video). In vehicle controls, neutrophils delayed the growth of *Candida* but were not efficient enough against clusters of *Candida* hyphae. These findings reveal the ability of HSA to improve the defensive functions of neutrophils isolated from immunocompromised patients with AD cirrhosis.

Supplementary video related to this article can be found at https://doi.org/10.1016/j.jhepr.2024.101184

Translational study in patients with AD cirrhosis receiving HSA as therapy

The study included 49 patients with AD cirrhosis at imminent risk of ACLF at entry (T1) who developed ACLF during the index hospitalization (T2) (Fig. S11A). Of the 49 patients, 30 received HSA between T1 and T2 (albumin group), and 19 remained free of HSA (non-albumin group). We assumed that investigating patients exhibiting the most severe forms of AD cirrhosis with the use of longitudinal data would limit the effect of interindividual variability on the assessment of HSA effects. The clinical characteristics and laboratory data of all patients at T1 and T2 are given in Table S3. Characteristics were similar in terms of standard laboratory values, including clinical differential blood counts for neutrophils, monocytes, and lymphocytes (Fig. S12A), which strongly correlated with RNA-seq-inferred blood counts (Fig. S12B). As expected, patients presented organ failures, higher white blood cell counts, and elevated levels of inflammatory markers at T2 compared with HV (Tables S3 and S4).

We next considered characteristics at T1 and T2 in patients in the albumin and non-albumin groups. In both groups, progression to ACLF from T1 to T2 was associated with significant increases in the model for end-stage liver disease (MELD) score. However, except for serum creatinine, which increased at T2, there were no significant within-group changes regarding the rest of longitudinally collected standard laboratory data and circulating levels of inflammatory mediators (Table 1). However, there were some in between-group differences. The delay between T1 and T2 was shorter in the albumin group than in the non-albumin group. Compared with patients in the non-albumin group, those in the albumin group had significantly higher CRP, IL-6, and IL-10 levels at T1 and higher Chronic Liver Failure Consortium organ failure (CLIF-C OF) score and creatinine, CRP, IL-6, and MCP-1 levels at T2. Moreover, a higher percentage of patients in the albumin group died by 28 and 90 days. The difference in survival was expected considering the higher prevalence of SBP and HRS-AKI in the albumin group.

Transcriptional characteristics of all patients at T1 and T2

Analyzing differentially expressed genes (DEGs) in two comparisons, T1 *vs*. HV and T2 *vs*. HV, we observed, as expected, strong similarities between the two disease stages. Thus, the number of DEGs was high in the two comparisons; that is, there were 4,615 DEGs in T1 relative to HV and 4,529 in T2 relative to HV. Of the 4,615 DEGs associated with T1, 3,929 (85%) overlapped with the DEGs assigned to T2 (Fig. S11B, top). By comparing effect-size changes in T1 *vs*. HV with T2 *vs*. HV, we observed a highly concordant magnitude of changes between the two signatures (Fig. S11B, bottom). Next, we used Quantitative Set Analysis for Gene Expression (QuSAGE) to analyze the differential expression of blood transcription modules (BTMs). Among the 258 annotated BTMs, the total number of DE BTMs (false discovery rate [FDR] <0.05) was 190 in T1 *vs*. HV and 186 in T2 *vs*. HV (Fig. S11C, top; Table S5A). These findings indicated extensive changes in the blood transcription module space in both T1 and T2. Strikingly, only 20 BTMs had specific differential expression relative to HV, in either T1 (12 modules) or T2 (eight modules), whereas 179 DE BTMs were shared with a concordant sign, of which 108 were upregulated

HSA exposure. (I) UMAP of 12,692 patients' $CD4^+$ T cells exposed to HSA and the vehicle, colored by cell types. (J) Overlay of HSA and vehicle exposure on $CD4^+$ T cell UMAP. (K) Box plots for the proportion of $CD4^+$ T cells that significantly changed after HSA exposure. Fig. 3A–C and F–K have been designed using scRNA-seq in PBMCs from nine patients with AD cirrhosis. (D) and (E) were designed based on results obtained by flow cytometry in PBMCs from 10 age-matched HV. Significant differences between groups were assessed using paired *t* tests. AD, acutely decompensated; HSA, human serum albumin; HV, healthy volunteers; PBMC, peripheral blood mononuclear cell; pDC, plasmacytoid dendritic cell; scRNA-seq, single-cell RNA sequencing; UMAP, Uniform Manifold Approximation and Projection.

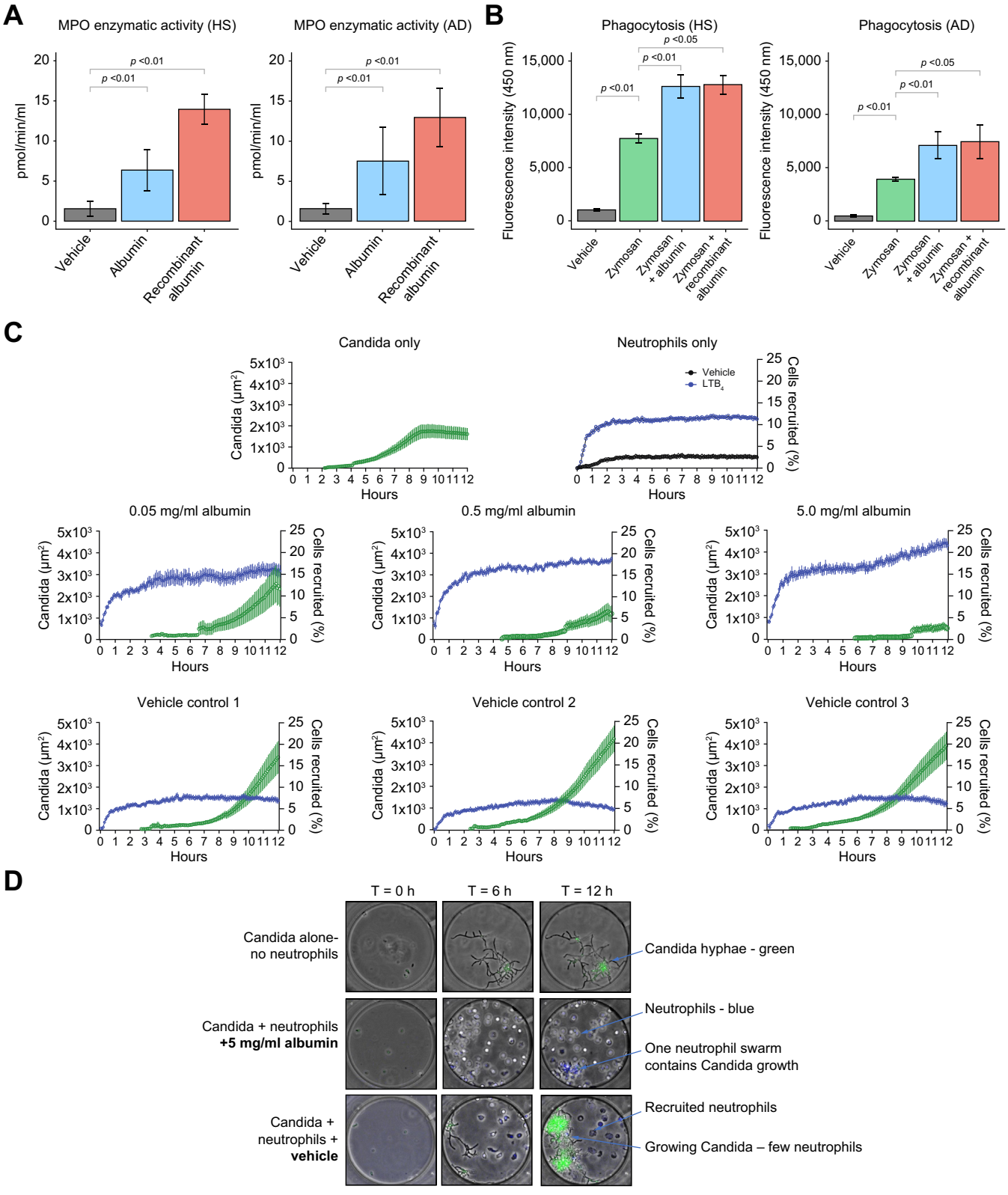

Fig. 4. Effects of HSA on the host defense function of neutrophils from patients with AD cirrhosis. (A) Neutrophils were incubated with cell medium (vehicle), HSA, or recombinant human albumin (both at 15 mg/ml) for 2 h at 37 °C in a 5% CO_2 incubator. Neutrophil degranulation was assessed by measuring the MPO enzymatic activity in the cell supernatants. (B) Phagocytic capacity assessed by incubating neutrophils with FITC-conjugated zymosan bioparticles alone or in the presence of HSA and recombinant albumin for 60 min and compared with vehicle control. (C) Quantification of *Candida albicans* growth and neutrophil recruitment in the microfluidic device. The size of *Candida* hyphae clusters was quantified based on the area of green fluorescence and is shown in green. The number of neutrophils recruited was quantified and shown in blue. For the neutrophils-only condition, we compared the neutrophils entering the chambers in the presence of the vehicle

and 71 downregulated (Table S5A). Fig. S11C (bottom) shows the 20 top gene modules for shared upregulated BTMs and 20 top gene modules for shared downregulated BTMs. Shared upregulated BTMs were related to innate immunity, including those related to Toll-like receptors and inflammatory signaling, interferon-alpha response, and innate immune cells (*i.e.* neutrophils, monocytes, and dendritic cells). Shared downregulated BTMs were related to T and NK cells and antigen presentation. These results were consistent with those obtained when analyzing gene signatures for the 10 main immune cell types (Fig. S13A) and 29 fine immune cell types (Fig. S13B). Collectively, our analyses of bulk blood RNA-seq data provided consistent results that highlighted the similarity of the transcriptional landscape in T1 and T2, both disease's stages being characterized by simultaneity between increases in gene signatures related to innate immunity and decreases in gene signatures related to adaptive immunity.

Whole blood gene signatures associated with HSA treatment

We compared differential gene expression between T2 and T1 for the albumin and non-albumin groups and found that gene signatures differed between the two groups. Indeed, 269 DEGs (92 upregulated, 177 downregulated) were specific for the albumin group, whereas 103 DEGs (64 upregulated, 39 downregulated) were specific for the non-albumin group; only 36 DEGs with a concordant sign were shared by the two groups (Fig. 5A). Identification of DEGs using volcano plots (Fig. 5B) illustrated the group specificity of both upregulated and downregulated genes. A broad variety of immunoglobulin genes (see below) and several major neutrophil genes (*CD177, OLFM4, PRG2, MPO, BPI, RETN, LCN2, CEACAM8, MCEMP1*) were upregulated in the albumin group (Fig. 5B, top), but not in the non-albumin group (Fig. 5B, bottom). These findings agree with the observed *in vitro* responses of B cells and neutrophils to albumin. Because analysis of DEGs drew our attention to immunoglobulin genes, we compared the effect-size changes between T2 and T1 within each group for each of the 125 genes (including 120 immunoglobulin genes) that are included in the Gene Ontology gene set labeled 'GOCC Immunoglobulin Complex'. We found that effect-size changes were greater in the albumin group (33 upregulated immunoglobulin genes) than in the non-albumin group (only 6) (Fig. 5C). Gene coding for constant regions of immunoglobulin heavy chains (*IGHM*, *IGHG2*, *IGHG3*, *IGHG4*, and *IGHA2*) were specifically upregulated in the albumin group. These findings are consistent with the results of SingleR analysis, which showed increases in gene signatures for plasmablasts that were specific for the albumin group (Fig. 5D, top). Immunoglobulin genes that were specifically upregulated in the albumin group also included genes for constant regions of immunoglobulin light chains kappa (*IGKC*) and lambda (*IGLC1*), genes for the V regions of the variable domain of immunoglobulin heavy chains, and genes for the V regions of the variable domain of light chains kappa and lambda. The three genes that were specifically upregulated in the non-albumin group were genes coding for the V regions of the variable domain of immunoglobulin heavy chains (Fig. 5C). Together these findings indicate an extensive upregulation of gene coding for immunoglobulins that were specific for patients who had received HSA.

Next, we applied QuSAGE to identify DE BTMs between T2 and T1 within each group. We first observed that the number of DE BTMs was greater in the albumin group than in the non-albumin group (36 *vs*. 6, respectively; Table S5B). Only one DE BTM, related to endoplasmic reticulum, was specifically upregulated in the non-albumin group (Fig. 5E). In sharp contrast, 31 DE BTMs (13 downregulated, 18 upregulated) were specific for the albumin group (Fig. 5E). Downregulated modules were related to erythropoiesis, cytoskeleton, or cell junction (Fig. 5E), whereas upregulated BTMs were related to activated dendritic cells, complement and other receptors in dendritic cells, cytokines, and chemokines (Fig. 5E). Upregulated BTMs specific for the albumin group also comprised modules related to B cells (including those related to enriched in B cells, plasma cells, and immunoglobulins), mismatch repair, cell cycle, and mitosis. Of note, upregulation of BTMs related to B cells in the albumin group was confirmed after adjusting the transcriptomics data by disease severity, as estimated by the MELD score (Fig. S14). Moreover, a direct and significant positive correlation was observed between the mean daily HSA dose administered to the patients and the expansion of the B cell compartment (Fig. S15). However, no evidence for HSA induction of NF-κB, a transcription factor involved in B-cell development and survival,[25,26] was observed in our study (Fig. S16). Of note, RNA-seq-inferred signatures for T and NK cells (Fig. 5D, middle and bottom panels; and Fig. S17A and B) as well as gene modules related to these cells (Table S5B), whose downregulation is a hallmark of patients with AD cirrhosis without and with ACLF (Fig. S11C), remained all downregulated among patients treated with HSA. Nevertheless, we observed that a BTM labeled 'mitotic cell cycle in stimulated $CD4^+$ T cells (M4.11)' was specifically upregulated among patients treated with HSA (Fig. 5E), which suggests some activation of transcription in $CD4^+$ T cells. Consistent with this, we found no overlap between member genes of the M4.11 BTM and genes used for SingleR analysis of $CD4^+$ T cells (Fig. S18). These findings were validated by scRNA-seq, in which the gene signature score for this BTM across all $CD4^+$ T cells computed using the Ucell package[27] showed a significantly higher cell density in HSA-treated cells relative to the vehicle (Fig. S19).

(black) with the number of neutrophils in the presence of LTB_4 chemoattractant (100 nM; blue). Twelve chambers per condition were quantified, and three of them are shown. (D) Microscopy images of neutrophil–*Candida albicans* interactions in microfluidic chambers. A similar number of *Candida* yeast was loaded in each chamber (time T-0). Neutrophils were loaded outside the chambers. Neutrophils migrated to the chambers, attracted by *Candida*-released molecules. In the presence of HSA, neutrophils actively phagocytosed *Candida*. Neutrophils swarmed around any *Candida* hyphae clusters, delaying their growth. In vehicle controls, neutrophils delayed the growth of *Candida* but were not efficient enough to contain clusters of *Candida* hyphae. (A)–(D) were designed using functional assays in freshly isolated peripheral neutrophils from six patients with AD cirrhosis and five age-matched HV. Significant differences between groups were assessed using paired *t* tests. AD, acutely decompensated; HSA, human serum albumin; HV, healthy volunteers; LTB_4, leukotriene B_4; MPO, myeloperoxidase.

Table 1. Characteristics of patients at time 1 (T1) and time 2 (T2) and deaths in the albumin and non-albumin groups.

	Albumin group (n = 30)		Non-albumin group (n = 19)		*p* value			
Characteristics	**T1**	**T2**	**T1**	**T2**	**T2 *vs.* T1 (albumin group)**	**T2 *vs.* T1 (non-albumin group)**	**T1 (between groups)**	**T2 (between groups)**
Markers of organ function								
MELD score, mean ± SD	19.2 ± 5.3	27.0 ± 6.6	19.0 ± 5.7	24.0 ± 7.5	<0.01	0.01	0.92	0.17
CLIF-C OF score, mean ± SD	7.0 ± 1.0	10.5 ± 2.6	7.4 ± 1.3	8.9 ± 1.5	<0.01	<0.01	0.26	0.01
Organ system failure, n (%)								
Liver failure	6 (20)	7 (23)	4 (21)	6 (32)	1	0.71	1	0.76
Kidney failure	0 (0)	23 (77)	0 (0)	13 (68)	<0.01	<0.01	1	0.76
Circulatory failure	0 (0)	10 (33)	1 (5)	1 (5)	<0.01	1	1	0.69
Cerebral failure	0 (0)	6 (20)	0 (0)	0 (0)	<0.01	1	0.82	0.31
Coagulation failure	0 (0)	4 (13)	0 (0)	4 (22)	0.12	0.10	1	0.01
Respiratory failure	0 (0)	9 (30)	0 (0)	0 (0)	<0.01	1	1	0.02
ACLF grade, no. (%)								
1	0 (0)	13 (43)	0 (0)	13 (72)	<0.01	<0.01	1	0.1
2–3	0 (0)	17 (57)	0 (0)	5 (28)	<0.01	0.05	1	0.1
Precipitating events, n (%)								
Infection as precipitant at T1 or T2	14 (47)	20 (67)	5 (26)	7 (37)	0.19	0.73	0.5	0.03
Alcohol-related hepatitis as precipitant at T1 or T2	14 (50)	14 (47)	7 (39)	7 (37)	1	1	0.4	0.21
Laboratory data								
International normalized ratio, median (IQR)	1.6 (1.4–1.7)	1.6 (1.5–2.0)	1.5 (1.2–1.8)	1.4 (1.3–2.2)	0.08	0.48	0.7	0.27
Total bilirubin (mg/L), median (IQR)	3.7 (2.0–9.0)	3.6 (2.4–11.3)	3.2 (1.3–9.5)	5.0 (1.0–13.5)	0.83	0.99	0.72	0.52
Serum creatinine (mg/dl), median (IQR)	1.2 (1.0–1.6)	2.7 (1.9–3.4)	1.4 (1.1–1.6)	2.1 (1.4–2.4)	<0.01	0.01	0.59	0.02
Serum sodium (mmol/L), mean ± SD	131 ± 5.8	133 ± -8.4	134.0 ± 6.9	132 ± 6.9	0.31	0.53	0.18	0.74
Serum albumin (g/dl), median (IQR)	2.6 (2.2–3.2)	3.0 (2.3–3.5)	2.7 (2.5–3.4)	3.0 (2.8–3.1)	0.21	0.36	0.23	0.89
White cell count (× 10^3/mm^3), median (IQR)	8.3 (7.0–10.3)	11.9 (6.2–13.7)	6.6 (4.6–8.6)	8.1 (5.8–12.4)	0.06	0.12	0.14	0.31
Absolute lymphocyte count (× 10^3/mm^3), median (IQR)	0.9 (0.6–1.3)	1.1 (0.7–1.6)	1.1 (0.8–1.5)	1.2 (0.8–1.8)	0.25	0.54	0.23	0.48
Absolute monocyte count (× 10^3/mm^3), median (IQR)	0.8 (0.6–1.1)	1.0 (0.6–1.3)	0.6 (0.3–1.0)	0.7 (0.6–0.9)	0.1	0.48	0.28	0.08
Absolute neutrophil count (× 10^3/mm^3), median (IQR)	6.1 (4.2–7.7)	8.9 (4.2–11.8)	4.0 (3.4–6.4)	4.5 (3.0–7.8)	0.12	0.73	0.15	0.05
C-reactive protein (mg/L), median (IQR)	31.3 (19.7–54.0)	33.5 (19.4–90.4)	13.3 (7.4–25.0)	16.1 (11.4–21.8)	0.5	0.69	<0.01	0.01
Blood levels of protein mediators of inflammation (pg/ml), median (IQR)								
Eotaxin	66.0 (43.9–97.1)	86.3 (58.6–104.1)	71.0 (43.7–121.0)	64.3 (50.1–121.9)	0.1	1	0.47	0.53
Granulocyte-colony stimulating factor	18.8 (4.4–43.2)	22.5 (9.0–73.8)	23.9 (7.6–99.6)	16.9 (3.6–70.9)	0.59	0.75	0.63	0.61
IFN-α2	10.0 (2.2–24.8)	16.8 (2.4–33.4)	12.8 (7.6–22.0)	17.6 (8.2–22.7)	0.43	0.5	0.68	0.97
IFN-γ	33.3 (7.0–86.0)	23.8 (12.1–97.2)	19.2 (7.2–98.7)	25.9 (7.9–45.8)	0.93	0.84	0.76	0.57
IL-1α	4.3 (1.7–7.2)	2.0 (0.8–6.1)	2.5 (1.1–3.3)	2.0 (0.3–3.9)	0.3	0.71	0.12	0.45
IL-1β	5.4 (3.1–10.8)	4.7 (2.3–13.0)	5.2 (1.8–9.7)	5.2 (1.9–8.7)	0.93	0.89	0.71	0.64
IL-6	24.7 (13.6–46.5)	52.5 (24.3–168.9)	9.3 (6.8–18.1)	16.9 (8.8–23.1)	0.16	0.1	<0.01	<0.01
IL-8	5.5 (3.5–10.7)	12.6 (4.0–18.1)	4.3 (2.6–13.0)	4.3 (1.0–9.0)	0.19	0.6	0.44	0.03

IL-10	10.0 (3.9–30.4)	13.1 (3.8–26.4)	2.4 (1.2–3.6)	4.7 (3.2–5.8)	0.97	0.08	0.03	0.15
Interferon-inducible protein 10	231 (123–374)	231 (169–615)	214 (166–482)	237 (141–487)	0.34	1	0.69	0.71
Monocyte chemoattractant protein 1	179 (147–257)	349 (230–533)	176 (158–279)	198.5 (100–281)	<0.01	0.8	0.74	<0.01
Macrophage inflammatory protein 1α	11.6 (8.4–23.5)	15.2 (9–28.9)	8.5 (2–18)	13.3 (4.5–19.4)	0.38	0.41	0.21	0.26
Macrophage inflammatory protein 1β	15.7 (11.7–19.7)	19.9 (13.8–30.6)	15.9 (12–22.7)	15.2 (11.7–19.6)	0.08	0.7	0.56	0.15
Tumor necrosis factor	30.8 (18.1–42)	35.3 (24–66.6)	37.6 (18.8–47.2)	35.6 (20.8–49.3)	0.31	0.89	0.59	0.62
Vascular endothelial growth factor	4.3 (0.8–8.2)	6.3 (2.6–16.4)	5.2 (1.9–12.7)	7.6 (4.7–11.7)	0.17	0.25	0.57	0.53

Normal values for blood inflammatory mediators are shown in Table S4. There was no significant difference between the albumin and non-albumin groups in terms of age (mean ± SD, 61.0 ± 7.9 and 59.1 ± 10.8 years, respectively) and number (%) of males (21 [70] and 12 [63], respectively). A higher percentage of patients in the albumin group than in the no-albumin group died by 28 days (30% [9/30] and 0%, respectively) and 90 days (67% [20/30] and 16% [3/19], respectively).
ACLF, acute-on-chronic liver failure; CLIF-C OF, Chronic Liver Failure Consortium organ failure; MELD, model for end-stage liver disease.

Discussion

The results of the current investigation contribute to understanding the mechanisms by which albumin administration is associated with a lower rate of infections and better survival in patients with AD cirrhosis. The investigation was performed *in vitro* in peripheral leukocytes and *in vivo* in patients with AD cirrhosis receiving albumin therapy. The investigation used cutting-edge technologies (*i.e.* bulk and scRNA-seq and swarming assays in microfluidic arenas) and gold-standard functional assays to assess leukocyte antimicrobial functions. The results of this investigation revealed that albumin modulates the peripheral immune system by attenuating B-cell depletion and revitalizing neutrophil functions in patients with AD cirrhosis.

To our knowledge, this is the first study to use longitudinal transcriptomics to characterize the effects of albumin on immune cells in patients with AD cirrhosis. The design of the study, particularly in those aspects related to the selection of patients, was performed after considering that patients hospitalized with ACLF, who are known to present an extremely dynamic clinical course with marked changes in the magnitude of systemic inflammation,[2,17] were clearly poor candidates for inclusion. Other phenotypes, including 'unstable' and 'stable' AD cirrhosis, were also not considered because they are associated with moderate systemic inflammation, which may further decrease during hospitalization, and we were interested in including only patients with intense systemic inflammation to better assess immune changes induced by albumin. For this reason, we chose patients with AD cirrhosis with imminent risk of developing ACLF, in whom the magnitude of systemic inflammation was similar to that seen in ACLF. We included only patients who received albumin for well-established indications (paracentesis, prevention of HRS-AKI associated with SBP, or HRS-AKI treatment)[12] even though this would introduce the bias of higher severity in patients receiving albumin. We did not select patients receiving albumin within 1 month before T1, those with a too-long interval between the two assessments of bulk blood RNA-seq, and those with a delay of >10 days between the last dose of albumin and T2. Finally, although albumin dosage and duration of treatment varied according to indications, we decided to analyze data in all patients irrespective of albumin dosage. The similarity of transcriptional characteristics as well as most clinical characteristics, standard laboratory values, and levels of cytokines in patients with AD cirrhosis before and after developing ACLF confirmed our assumption that patients included in the study were in a relatively steady state of systemic inflammation during the study.

The major finding of the scRNA-seq and bulk RNA-seq in blood cells from patients with AD cirrhosis was that albumin administration triggered signals that caused an expansion of the B cell compartments, and likely the $CD4^+$ T cell compartments, while activating some mononuclear myeloid cells. These findings are extremely relevant, considering that the prevalence of bacterial infections at admission in patients with AD cirrhosis is very high (37.3 and 25.1% in patients with and without ACLF, respectively).[10,28] Among the uninfected patients at admission, 46% with and 18% without ACLF develop bacterial infection during hospitalization. The existence of a profound impairment of the innate immune system, which is highlighted by impaired neutrophil and monocyte antimicrobial functions and lymphocyte depletion, likely explains such a high

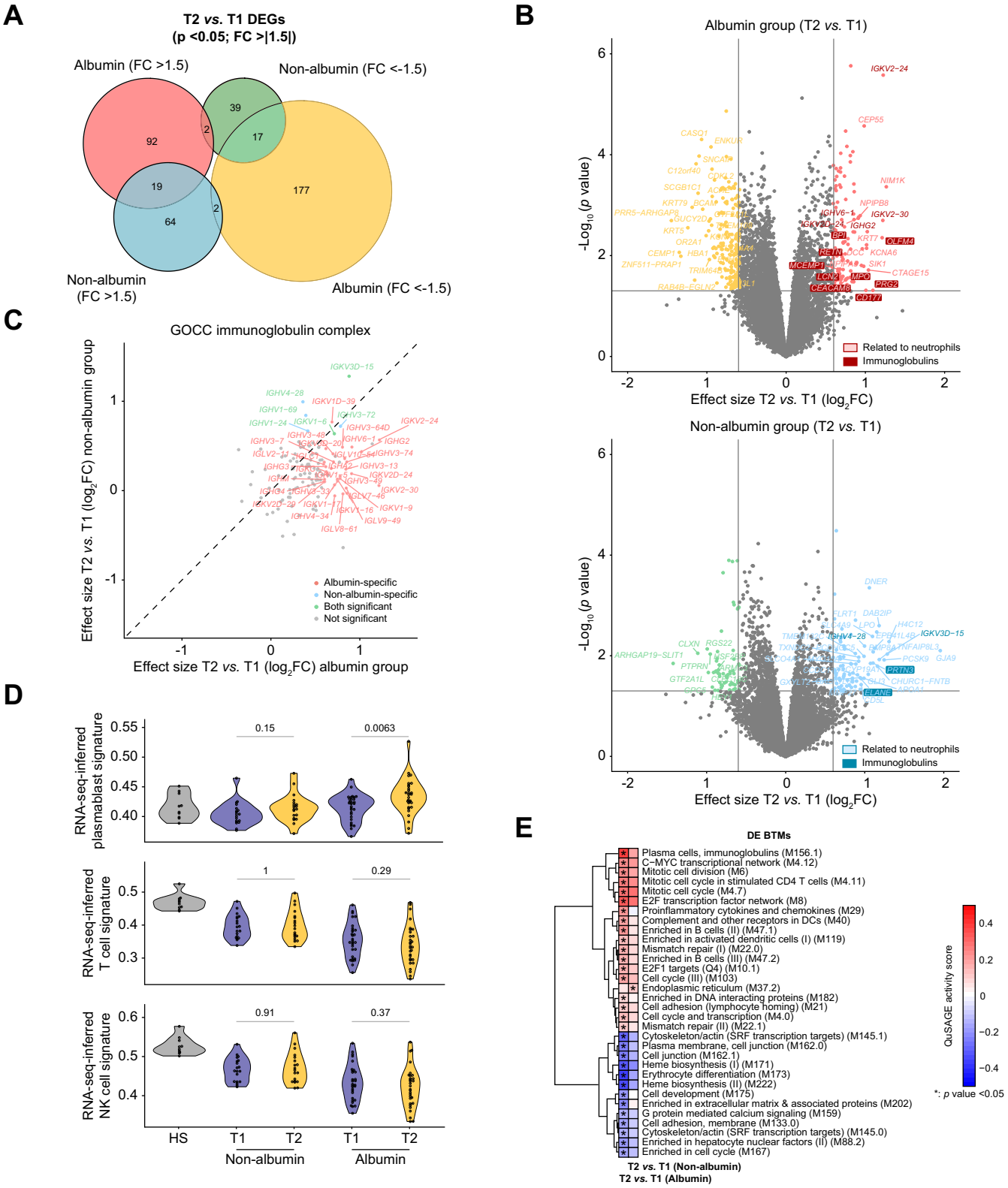

Fig. 5. Whole blood gene signatures associated with HSA treatment. (A) Euler plot showing DEGs between T2 and T1 for the albumin and non-albumin groups. *DEGs were defined by an* absolute FC greater than 1.5 and p <0.05. (B) Volcano plots showing differential expression effect size (log_2 FC) between T2 and T1 plotted against significance ($-log_{10}$ p) for the albumin (top) and non-albumin (bottom) groups. In both volcano plots, gray points indicate genes with no significant difference in expression between T2 and T1 (with absolute FC <1.5 and p >0.05, i.e. $-log_{10}$ p <1.3). Colored points indicate DEGs, either upregulated or downregulated. The neutrophil-related genes are highlighted. (C) Differential expression effect size (log_2 FC) between T2 and T1 in the albumin group compared with corresponding differential effect size in the non-albumin group. Only genes included in the Gene Ontology gene set 'GOCC_Immunoglobulin Complex' are shown here. DEGs with a concordant sign were considered as shared. (D) Violin plots of RNA-seq inferred signatures at T1 and T2 for plasmablasts, NK cells, and T cells, determined using the

risk of infections in these patients.[29] Of note, because changes in immune-cell transcriptome seen after albumin administration occurred in the absence of changes in albuminemia, the effects of albumin on the transcriptome of immune cells cannot be merely explained by correction of hypoalbuminemia but rather by qualitative differences between the 'commercial' albumin and the circulating endogenous albumin in patients with AD cirrhosis, which is known to be post-translationally modified and highly oxidized.[30]

Some mechanisms could explain the effect of albumin on immune cells. Immune cells can be activated by osmotic stress.[31] Therefore, the movement of water from cells to the extracellular milieu (osmotic stress) could be a mechanism by which albumin exerted immunomodulatory effects in our *in vitro* cell experiments. However, we did not see the same response in PBMCs incubated with mannitol, a compound sharing the iso-oncotic properties of albumin. Another mechanism could be the induction of NF-κB, a master transcription factor in B cells[25] that has been reported to be activated by albumin in a human renal proximal tubule-derived cell line.[26] However, in our study, we did not find any sign of NF-κB induction in response to albumin. Because extracellular acidification is known to reprogram immune cell responsiveness,[32] another possibility is that a change in pH caused by albumin, which is a highly soluble acidic molecule, could account for the activation of immune cells. This can also occur at the intracellular level because albumin is rapidly internalized by mononuclear myeloid cells[16] and intracellular acidification results in changes in immune cell performance.[33] In contrast, the interaction of albumin with FcRn or with voltage-gated proton channels, which leads to stimulation of phagocytosis and degranulation,[19,34,35] respectively, could mechanistically explain the activation of neutrophil antimicrobial function by albumin. In this regard, we observed that the immunostimulatory actions of albumin in mononuclear leukocytes were partially inhibited by an antibody blocking FcRn.

This study has some limitations. First, there is a difference in severity between the two study groups. Second, our results are mostly descriptive, which makes it difficult to directly prove immune restoration by albumin. The third limitation is related to the study design. Indeed, we leveraged the prespecified collection of blood for RNA-seq in patients of the PREDICT study at admission (when they did not have ACLF) and at the time of ACLF development to identify patients who did or did not receive albumin during the progression to ACLF. Thus, we do not report the results of a controlled study specifically designed to investigate the effects of prespecified systematic albumin administration, for example, on the development of ACLF. The ideal protocol would consist in daily administration of albumin with the objective of, for example, maintaining blood levels of albumin above 3.0 g/dl, as in the ATTIRE trial.[36] Nevertheless, it is noteworthy that conducting a prospective randomized controlled trial of albumin for preventing ACLF in patients who present with pre-ACLF would face major methodological issues. Indeed, there are currently no criteria to identify patients with pre-ACLF among those who present for AD cirrhosis.[17] Therefore, performing randomized controlled trials that enroll well-matched patients with AD cirrhosis is a big challenge, and criteria for stratifying patients according to the risk of ACLF is an unmet medical need.

In conclusion, the results of this study suggest that albumin promotes the expansion of the B cell compartment and improves neutrophil antimicrobial functions. These findings contribute to understanding the clinical benefits of albumin therapy such as reducing the incidence rate of infections in patients with AD cirrhosis.[13]

Affiliations

[1]*European Foundation for the Study of Chronic Liver Failure (EF CLIF), European Association for the Study of the Liver (EASL)–CLIF Consortium, and Grifols Chair, Barcelona, Spain;* [2]*Hospital Clínic-IDIBAPS, Barcelona, Spain;* [3]*CIBER of Hepatic and Digestive Diseases (CIBERehd); Barcelona, Spain;* [4]*Universitat de Barcelona, Barcelona, Spain;* [5]*Centre Nacional d'Anàlisi Genòmica (CNAG), Barcelona, Spain;* [6]*Translational Clinical Research Program, Institute "Hospital del Mar" for Medical Investigations (IMIM), Barcelona, Spain;* [7]*Institut National de la Santé et de la Recherche Médicale (INSERM), Université Paris-Cité, Centre de Recherche sur l'Inflammation (CRI), Paris, France;* [8]*Assistance Publique–Hôpitaux de Paris (AP-HP), Hôpital Beaujon, Département d'Anesthésie et de Réanimation, DMU Parabol, Clichy, France;* [9]*Department of Internal Medicine B, University of Münster, Münster, Germany;* [10]*Institute for Research in Biomedicine (IRB), Barcelona, Spain;* [11]*Center for Engineering in Medicine and Surgery, Massachusetts General Hospital, Shriners Burns Hospital, Harvard Medical School, Boston, MA, USA;* [12]*Center for Cooperative Research in Biosciences (CIC bioGUNE), Parque Tecnológico de Bizkaia, Derio, Spain;* [13]*Department of Medical and Surgical Sciences, University of Bologna, Bologna, Italy;* [14]*Liver Failure Group, Institute for Liver Disease Health, University College London, Royal Free Hospital, London, UK;* [15]*Unit of Internal Medicine and Hepatology (UIMH), Department of Medicine – DIMED, University of Padova, Padova, Italy;* [16]*Immunology Unit, Faculty of Medicine and Health Sciences, University of Barcelona, Barcelona, Spain;* [17]*Catalan Institute for Research and Advanced Studies (ICREA); Barcelona, Spain;* [18]*Assistance Publique – Hôpitaux de Paris (AP-HP), Hôpital Beaujon, Service d'Hépatologie, Clichy, France*

Abbreviations

ACLF, acute-on-chronic liver failure; AD, acutely decompensated; BTM, blood transcription module; DE, differentially expressed; DEG, differentially expressed genes; FC, fold change; FcRn, neonatal Fc receptor; FDR, false discovery rate; GSEA, gene set enrichment analysis; HRS-AKI, hepatorenal syndrome–acute kidney injury; HSA, human serum albumin; HV, healthy volunteers; MELD, model for end-stage liver disease; MPO, myeloperoxidase; NES, normalized enrichment score; NK, natural killer; PBMC, peripheral blood mononuclear cell; QuSAGE, Quantitative Set Analysis for Gene Expression; RNA-seq, RNA sequencing; SBP, spontaneous bacterial peritonitis; scRNA-seq, single-cell RNA sequencing; UMAP, Uniform Manifold Approximation and Projection.

SingleR software, in the albumin and non-albumin groups. Baseline values in HV are also shown. Values of *p* are from Kruskal–Wallis tests. (E) Heat map of 32 DE BTMs between T2 and T1 that were specific for either the albumin or non-albumin group. Thirty-one DE BTMs were specific for the albumin group, whereas only one DE BTM ('endoplasmic reticulum [M37.2]') was specific for the non-albumin group. BTMs were hierarchically clustered based on QuSAGE activity scores obtained in the albumin group. Asterisks denote p <0.05 obtained when comparing probability density functions with QuSAGE. Color represents QuSAGE activity score. BTM, blood transcription module; DE, differentially expressed; DEG, differentially expressed gene; FC, fold change; HSA, human serum albumin; NK, natural killer; QuSAGE, Quantitative Set Analysis for Gene Expression; RNA-seq, RNA sequencing; T1, time 1; T2, time 2.

Financial support

This research was supported by EF CLIF, a private, non-profit organization receiving unrestricted grants from Grifols and Fundació Privada Cellex. EF CLIF is a partner and/or coordinator of several European Union (EU) Horizon 2020 program projects (Nos. 825694 and 847949). This study was also supported by Ministerio de Ciencia e Innovacion/Agencia Estatal Investigación MCIN/AEI, PID2022-138970OB-I00 10.13039/501100011033/FEDER, UE (to JC) and RTI2018-093894-B-I00 (to AC). LJ-G has held an FPU PhD fellowship (FPU19/04886) from the Spanish Ministry of Science, Innovation and Universities. EW was an EF CLIF Research Fellow who received grants from Fundació Privada Cellex and the Fondation Bettencourt-Schueller. IH received a Marie Skłodowska-Curie grant agreement (No. 75451) from the EU's Horizon 2020 Research and Innovation Program. The funders had no influence on the study design, data collection and analysis, decision to publish, or preparation of the manuscript.

Conflicts of interest

MB is part of the speakers' bureau for Grifols SA, Octapharma AG, Shire/Takeda, CLS Behring GmbH, and PPTA and is a consultant for Grifols SA, CLS Behring GmbH, Martin Pharmaceuticals, and Shire/Takeda. HH is a co-founder and shareholder of Omniscope, a scientific advisory board member of MiRXES, and a consultant to Moderna. RJ has research collaborations with Yaqrit and Takeda. He is the inventor of OPA, which has been patented by UCL and licensed to Mallinckrodt Pharma. He is also the founder of Yaqrit Ltd, a spin-out company from University College London and Thoeris Ltd. JCN is a scientific consultant of Omniscope. The remaining authors disclose no conflicts.

Please refer to the accompanying ICMJE disclosure forms for further details.

Authors' contributions

Study concept and design: VA, RM. Acquisition of data and sample measurements: MC, CLV, BRG, XM, AV, AMA, EW, JT, JF, MB, RJ, PA. Bioinformatic and statistical analyses: JJL, IH, FA, LJG, JCN, AMA, DM. Drafting of the manuscript: JC, VA, RM. Critical revision of the manuscript for important intellectual content: EW, JC, JJL, IH, JT, FA, JF, LJG, JCN, AV, AMA, MB, RJ, PA, GM, AC, HH. Study supervision: RM, VA, HH.

Data availability statement

All data associated with this work is presented in the main manuscript or Supplementary material. For availability of any other type of data, contact the corresponding authors.

Acknowledgements

We thank Dr Anna Bosch, Dr Lidia García-Campmany, Ms Anna Curto, Ms Cristina Sanchez, and Mr Alex Amoros for their help.

Supplementary data

Supplementary data to this article can be found online at https://doi.org/10.1016/j.jhepr.2024.101184.

References

Author names in bold designate shared co-first authorship

[1] Moreau R, Jalan R, Ginès P, et al. Acute-on-chronic liver failure is a distinct syndrome that develops in patients with acute decompensation of cirrhosis. Gastroenterology 2013;144:1426–1437.
[2] Arroyo V, Moreau R, Jalan R. Acute-on-chronic liver failure. N Engl J Med 2020;382:2137–2145.
[3] **Weiss E**, **de la Grange P**, Defaye M, et al. Characterization of blood immune cells in patients with decompensated cirrhosis including ACLF. Front Immunol 2021;11:619039.
[4] **Clària J**, **Stauber RE**, Coenraad MJ, et al. Systemic inflammation in decompensated cirrhosis: characterization and role in acute-on-chronic liver failure. Hepatology 2016;64:1249–1264.
[5] López-Vicario C, Checa A, Urdangarin A, et al. Targeted lipidomics reveals extensive changes in circulating lipid mediators in patients with acutely decompensated cirrhosis. J Hepatol 2020;73:817–828.
[6] Bernsmeier C, Pop OT, Singanayagam A, et al. Patients with acute-on-chronic liver failure have increased numbers of regulatory immune cells expressing the receptor tyrosine kinase MERTK. Gastroenterology 2015;148:603–615.
[7] Korf H, du Plessis J, van Pelt J, et al. Inhibition of glutamine synthetase in monocytes from patients with acute-on-chronic liver failure resuscitates their antibacterial and inflammatory capacity. Gut 2019;68:1872–1883.
[8] O'Brien AJ, Fullerton JN, Massey KA, et al. Immunosuppression in acutely decompensated cirrhosis is mediated by prostaglandin E_2. Nat Med 2014;20:518–523.
[9] Stadlbauer V, Mookerjee RP, Wright GA, et al. Role of Toll-like receptors 2, 4, and 9 in mediating neutrophil dysfunction in alcoholic hepatitis. Am J Physiol Gastrointest Liver Physiol 2009;296:G15–G22.
[10] Fernández J, Acevedo J, Wiest R, et al. Bacterial and fungal infections in acute-on-chronic liver failure: prevalence, characteristics and impact on prognosis. Gut 2018;67:1870–1880.
[11] **Fernández J**, **Piano S**, **Bartoletti M**, et al. Management of bacterial and fungal infections in cirrhosis: the MDRO challenge. J Hepatol 2021;75:101–117.
[12] European Association for the Study of the Liver. EASL Clinical Practice Guidelines for the management of patients with decompensated cirrhosis. J Hepatol 2018;69:406–460.
[13] Caraceni P, Riggio O, Angeli P, et al. Long-term albumin administration in decompensated cirrhosis: an open-label randomised trial. Lancet 2018;391:2417–2429.
[14] **Fernández J**, **Clària J**, Amorós A, et al. Effects of albumin treatment on systemic and portal hemodynamics and systemic inflammation in patients with decompensated cirrhosis. Gastroenterology 2019;157:149–162.
[15] Bihari S, Bannard-Smith J, Bellomo R. Albumin as a drug: its biological effects beyond volume expansion. Crit Care Resusc 2020;22:257–265.
[16] Casulleras M, Flores-Costa R, Duran-Güell M, et al. Albumin internalizes and inhibits endosomal TLR signaling in leukocytes from patients with decompensated cirrhosis. Sci Transl Med 2020;12:eaax5135.
[17] Trebicka J, Fernandez J, Papp M, et al. The PREDICT study uncovers three clinical courses of acutely decompensated cirrhosis that have distinct pathophysiology. J Hepatol 2020;73:842–854.
[18] Ellett F, Jalali F, Marand AL, et al. Microfluidic arenas for war games between neutrophils and microbes. Lab Chip 2019;19:1205–1216.
[19] Pyzik M, Rath T, Lencer WI, et al. FcRn: the architect behind the immune and nonimmune functions of IgG and albumin. J Immunol 2015;194:4595–4603.
[20] Stewart A, Ng JC, Wallis G, et al. Single-cell transcriptomic analyses define distinct peripheral B cell subsets and discrete development pathways. Front Immunol 2021;12:602539.
[21] Polet H, Spieker-Polet H. Serum albumin is essential for in vitro growth of activated human lymphocytes. J Exp Med 1975;142:949–959.
[22] Kapellos TS, Bonaguro L, Gemünd I, et al. Human monocyte subsets and phenotypes in major chronic inflammatory diseases. Front Immunol 2019;10:2035.
[23] Grieshaber-Bouyer R, Radtke FA, Cunin P, et al. The neutrotime transcriptional signature defines a single continuum of neutrophils across biological compartments. Nat Commun 2021;12:2856.
[24] Amulic B, Cazalet GL, Hayes KD, et al. Neutrophil function: from mechanisms to disease. Annu Rev Immunol 2012;30:459–489.
[25] Sasaki Y, Iwai K. Roles of the NF-κB pathway in B-lymphocyte biology. Curr Top Microbiol Immunol 2016;393:177–209.
[26] Drumm K, Bauer B, Freudinger R, et al. Albumin induces NF-κB expression in human proximal tubule-derived cells (IHKE-1). Cell Physiol Biochem 2002;12:187–196.
[27] Andreatta M, Carmona SJ. UCell: robust and scalable single-cell gene signature scoring. Comput Struct Biotechnol J 2021;19:3796–3798.
[28] Trebicka J, Fernandez J, Papp M, et al. PREDICT identifies precipitating events associated with the clinical course of acutely decompensated cirrhosis. J Hepatol 2021;74:1097–1108.
[29] Arroyo V, Moreau R, Kamath PS, et al. Acute-on-chronic liver failure in cirrhosis. Nat Rev Dis Primers 2016;2:16041.
[30] Alcaraz-Quiles J, Casulleras M, Oettl K, et al. Oxidized albumin triggers a cytokine storm in leukocytes through P38 mitogen-activated protein kinase: role in systemic inflammation in decompensated cirrhosis. Hepatology 2018;68:1937–1952.
[31] Ip WK, Medzhitov R. Macrophages monitor tissue osmolarity and induce inflammatory response through NLRP3 and NLRC4 inflammasome activation. Nat Commun 2015;6:6931.
[32] Jiang W, Le J, Wang PY, et al. Extracellular acidity reprograms macrophage metabolism and innate responsiveness. J Immunol 2021;206:3021–3031.
[33] Murase M, Kawasaki T, Hakozaki R, et al. Intravesicular acidification regulates lipopolysaccharide inflammation and tolerance through TLR4 trafficking. J Immunol 2018;200:2798–2808.
[34] Vidarsson G, Stemerding AM, Stapleton NM, et al. FcRn: an IgG receptor on phagocytes with a novel role in phagocytosis. Blood 2006;108:3573–3579.

[35] Zhao R, Dai H, Arias RJ, et al. Direct activation of the proton channel by albumin leads to human sperm capacitation and sustained release of inflammatory mediators by neutrophils. Nat Commun 2021;12:3855.

[36] China L, Freemantle N, Forrest E, et al. A randomized trial of albumin infusions in hospitalized patients with cirrhosis. N Engl J Med 2021;384:808–817.

Keywords: Multiorgan failure; Inflammation; Immunosuppression; Gene expression.
Received 27 December 2023; received in revised form 26 July 2024; accepted 31 July 2024; Available online 8 August 2024

Journal of Hepatology, Volume *6*

Supplemental information

Albumin reprograms the B cell transcriptional landscape and improves neutrophil antimicrobial function in patients with decompensated cirrhosis

Joan Clària, Ferran Aguilar, Juan-José Lozano, Laura Jiménez-Gracia, Juan C. Nieto, Berta Romero-Grimaldo, Xavi Marcos-Fa, Emma Giarracco, Emmanuel Weiss, Jonel Trebicka, Inmaculada Hernàndez, Javier Fernandez, Mireia Casulleras, Cristina López-Vicario, Sinan Muldur, Alex Hopke, Alexandru Vlagea, Ana M. Aransay, Domenica Marchese, Mauro Bernardi, Rajiv Jalan, Paolo Angeli, Giuliana Magri, Andrea Cerutti, Daniel Irimia, Holger Heyn, Vicente Arroyo, and Richard Moreau

Albumin reprograms the B cell transcriptional landscape and improves neutrophil antimicrobial function in patients with decompensated cirrhosis

Joan Clària, Ferran Aguilar, Juan-José Lozano, Laura Jiménez-Gracia, Juan C. Nieto, Berta Romero-Grimaldo, Xavi Marcos-Fa, Emma Giarracco, Emmanuel Weiss, Jonel Trebicka, Inmaculada Hernàndez, Javier Fernandez, Mireia Casulleras, Cristina López-Vicario, Sinan Muldur, Alex Hopke, Alexandru Vlagea, Ana M. Aransay, Domenica Marchese, Mauro Bernardi, Rajiv Jalan, Paolo Angeli, Giuliana Magri, Andrea Cerutti, Daniel Irimia, Holger Heyn, Vicente Arroyo, Richard Moreau

Table of contents

Supplementary methods……2

Supplementary figures……17

Supplementary tables……39

Table S5……separate excel file

Supplementary video……..separate avi file

Supplementary video legend……45

Supplementary references……..46

Supplementary methods

Selection of Patients from the PREDICT Study

The PREDICT study was a large-scale prospective observational multicenter investigation aimed to identify precipitants and short-term (3-month) clinical course phenotypes in patients hospitalized for acutely decompensated (AD) cirrhosis without acute-on-chronic liver failure (ACLF) (*1*). AD cirrhosis was defined by the acute development of ascites, encephalopathy and/or gastrointestinal hemorrhage (*1*), according to previous studies (*2,3*). AD cirrhosis develops in the context of intense systemic inflammation (*2-5*). ACLF is the extreme expression of AD cirrhosis and is characterized by extrahepatic organ failure(s) and high short-term mortality (*2,3*). The PREDICT study consisted of a prespecified longitudinal collection of clinical and standard laboratory data and biological samples, including whole-blood for RNA-seq. Investigators used an electronic clinical-report form to report clinical data, including treatments and standard laboratory data (*1*). Data were continuously monitored on-line by the Data Management Center of the European Foundation for the Study of Chronic Liver Failure. Among patients of the PREDICT study, three distinct clinical phenotypes were identified according to the clinical course. Approximately 20% of the patients had pre-ACLF at enrollment because these patients developed ACLF within 3 months. It was the group with the highest grade of systemic inflammation at enrollment. The other two clinical phenotypes (unstable and stable decompensated cirrhosis) included patients with lower grade of systemic inflammation, which may rapidly improve under standard medical therapy (*1*). Unfortunately, among patients admitted for AD cirrhosis without ACLF, there are currently no available markers enabling to distinguish those who will develop ACLF from those who will not develop this complication (1). Therefore, it is currently not possible to design studies, interventional, in which the inclusion criterion would be the presence of AD cirrhosis at imminent risk of ACLF. For this reason, prospective observational studies are of most interest in the assessment of

treatments in these patients.

The selection of patients from PREDICT followed this criteria: i) all AD patients were at imminent risk of ACLF at enrollment (T1) and developed ACLF during the index hospitalization (T2); ii) in all patients, bulk blood RNA-seq data were obtained at T1 and T2; iii) None of the forty-nine patients had received albumin before T1; iv) Thirty out of the forty-nine patients had received albumin between T1 and T2 and composed the albumin group whereas the nineteen others remained free of albumin between T1 and T2 and composed the non-albumin group. In the albumin group, the median time between T1 and T2 for blood collections for RNA-seq was 11.5 days (interquartile range [IQR], 6.2-18.7). The median duration of HSA treatment was 2.5 days (IQR, 2-6) and the dose was 40.0 g per day (IQR, 22.5-57.5). The time between the last HSA administration and subsequent blood collection was 1.5 days (IQR, 0.0-2.7), indicating that we explored patients soon after HSA administration. In the non-albumin group, the median time between T1 and T2 was 29 days (IQR, 16-52). The 60 first patients with AD cirrhosis and imminent risk of ACLF enrolled in the PREDICT study were eligible. Of these, 11 (9 who had received albumin prior baseline transcriptomics and 2 showing poor-quality control in the transcriptomic analysis) were excluded. The *in vivo* study was therefore performed in 49 patients. The electronic case-reports form of the PREDICT study prespecified the following indications for intravenous albumin: large-volume therapeutic paracentesis, spontaneous bacterial peritonitis, hepatorenal syndrome-acute kidney injury, and other indication. Among the 30 patients who had received intravenous albumin between enrollment and ACLF development and were analyzed in the present study (**Fig. S11A**), the primary indications for albumin were large-volume therapeutic paracentesis, spontaneous bacterial peritonitis, and hepatorenal syndrome-acute kidney injury (HRS-AKI, formerly type 1 hepatorenal syndrome).

Immunophenotyping

Extended phenotyping of blood immune cells was performed by flow cytometry using the following panels of antibodies (clones are indicated within brackets): TBNK panel including CD4 (SK3), CD56 (MY31), CD8 (RPA-T8), CD16 (3G8), CD14, CD45 (2D1), CD3 (SP34-2) and CD19 (SJ25C1); B cell panel including CD21 (B-ly4), IgD (IA6-2), CD24 (ML5), CD38 (HIT2), CD27 (M-T271), CD45 (2D1), IgM (G20-127) and CD19 (SJ25C1); dendritic cell panel including CD3 (SK7), CD16 (3G8), CD19 (SJ25C1), CD20 (L27), CD14 (MφP9), CD56 (NCAM16.2), CD1c (F10), CD123 (7G3), CD11c (B-ly6), CD34 (8G12) + CD117 (YB5.B8), CD45 (2D1), HLA-DR (L243) and CD141 (1A4); and T regulatory cell panel including HLA-DR (L243), CD25 (M-A251), CD127 (HIL-7R-M21), CD45RO (UCHL1), CD3 (SK7), CD4 (L200) and CCR4 (1G1). All antibodies were purchased at BD Biosciences (San Jose, CA). For immunophenotyping, the antibodies were titrated and used to stain 100 µL of EDTA-collected whole blood during 20 minutes in the dark. Then erythrocytes were lysed by incubating 20 minutes with BD FACS™ lysing solution and washed twice. After lysis, the cells were resuspended in phosphate-buffered saline. After compensation, data acquisition was performed with a BD FACSCanto II flow cytometer (Becton Dickinson, Franklin Lakes, NJ). For analysis BD FACSDiva (Becton Dickinson) software was used. A minimum of 100,000 total events were acquired. The graphical layout was created using the FlowJo software (Becton Dickinson).

Immunophenotyping and isolation of PBMCs

To assess changes in B cell phenotypes induced by albumin, PBMCs from ten healthy subjects were isolated and seeded at a density of $3x10^6$ cells/ml in RPMI 1640 medium with BAFF (Enzo Life Sciences, Farmingdale, NY) (10 ng/ml) as a survival factor, with or without albumin (15 mg/ml) and incubated at 37ºC, 5% CO_2 for 24 hours. At the end of the incubation period, cells were centrifuged at 400 g for 5 min and resuspended in cold DPBS. Then, cells were incubated for 30 min with the LIVE/DEAD yellow viability marker (L34959, Thermo Fisher

Scientific), and washed with PBS. Thereafter, cells were stained in MACS buffer (pH 7.4) for 20 min with the following anti-human antibodies:

Antigen	Isotype	Conjugated dye	Reference	Company
CD10	Mouse IgG1, κ	BV421	312217	Biolegend (San Diego, CA)
CD19	Mouse IgG1, κ	Pacific Blue	302224	Biolegend
CD24	Mouse IgG2a, κ	PE-Cy7	311120	Biolegend
CD27	Mouse IgG1, κ	BV650	302827	Biolegend
CD38	Mouse IgG1, κ	APC-Fire810	CUSTOM	Biolegend
IgD	Goat F(ab')2 IgG	FITC	2032-02	Southern Biotech (Birmingham, AL)

After washing with PBS, the cells were fixed with paraformaldehyde at 4% for 12 min and then washed again with PBS. Finally, cells were resuspended in 250 µl of cold PBS. The analysis was performed on a Cytek Aurora spectral flow cytometer (Cytek Biosciences, Fremont, CA).

PBMC and neutrophil isolation

Peripheral venous blood (20 ml) was obtained by venipuncture and collected into EDTA-coated, sterile, pyrogen-free tubes (Becton Dickinson). Blood samples were centrifuged at 200 g for 10 min and sedimented cells were diluted with DPBS without calcium and magnesium ($DPBS^{--}$) up to a volume of 20 ml. Diluted blood was layered over 13.3 ml of Ficoll-Hypaque and centrifuged at 500 g for 25 min with the break-off. PBMCs obtained from the mononuclear cell layer were then incubated with pre-warmed ammonium-chloride-potassium lysis buffer for 10 min at room temperature to remove red blood cells and then centrifuged at 400 g for 5 min. The resultant pellet was washed with $DPBS^{--}$. Isolated PBMCs were re-suspended in RPMI 1640 medium containing penicillin (100 U/ml), streptomycin (100 U/ml), and L-glutamine (4 mM) without fetal bovine serum (FBS) and viable cells were then automatically counted. After 30 minutes of resting, $3x10^6$ viable cells were incubated at 37°C and used for bulk and scRNA-seq. Neutrophils were also isolated using the Ficoll-Hypaque method described above. Briefly,

after separation of the PBMC layer in the supernatant, neutrophils were collected from the pellet and incubated with pre-warmed ammonium-chloride-potassium lysis buffer for 10 min at room temperature to remove red blood cells and then centrifuged at 400 g for 5 min. The red blood lysis procedure was repeated twice, and the resultant pellet was washed with $DPBS^{--}$. Isolated neutrophils were resuspended in RPMI 1640 medium containing penicillin, streptomycin, and L-glutamine without FBS and used in the assays. For the chemotaxis and swarming assays, blood samples from healthy donors were purchased from RBC components (Alston, MA) and neutrophils were isolated from the blood using the STEMCELL direct neutrophil isolation kit (Vancouver, Canada), according to the manufacturer's protocols. Isolated neutrophils were counted and re-suspended in Iscove's Modified Dulbecco's Medium (IMDM).

scRNA-seq in PBMCs

PBMCs were seeded in RPMI 1640 medium at a density of $1.5x10^6$ cells/ml and incubated with either human serum albumin (Albutein®) (15 mg/ml) or vehicle (culture medium) for two hours at 37ºC in a 5% CO_2 incubator. At the end of the incubation period, cells were rapidly (within 30 min) transferred on ice to the Single Cell Genomics platform from the CNAG. PBMCs were centrifuged for 5 min at 500 g at 4°C. The supernatant was removed, and the pellet was re-suspended in 1xPBS supplemented with 0.05% BSA. Samples were filtered with a 40-µm strainer (pluriSelect) and cell concentration and viability were verified by counting with a TC20™ Automated Cell Counter (Bio-Rad Laboratories, Hercules, CA). PBMC samples from two patients and two healthy subjects were directly used for cell partition into Gel Bead in Emulsion with a Target Cell Recovery of 5,000 cells each. For all the other cases, donor matched albumin or vehicle samples were labeled by cell hashing and pooled in one 10x Genomics channel to avoid technical biases. Cell hashing was performed following the manufacturer's instructions (Cell hashing and Single Cell Proteogenomics Protocol Using

TotalSeq™ Antibodies; BioLegend, San Diego, CA). Briefly, for each sample, 1-2 million cells were re-suspended in 100 µl of Cell Staining Buffer (BioLegend) and incubated for 10 min at 4ºC with 5 µl of Human TruStain FcX™ Fc Blocking reagent (BioLegend). Next, a specific TotalSeq-A antibody-oligo conjugate (anti-human Hashtag 1-4, Biolegend) was added to each of the two conditions (albumin and vehicle) and incubated on ice for 30 min. Cells were then washed three times with cold PBS-0.05% BSA and centrifuged for 5 min at 500 g at 4°C. Finally, cells were re-suspended in an appropriate volume of 1xPBS-0.05% BSA to obtain a final cell concentration 500-1000 cells/µl, suitable for 10x Genomics scRNA-seq. An equal volume of hashed cell suspension from each of the two conditions was mixed and filtered with a 40-µm strainer. Cell concentration was verified by counting with a TC20™ Automated Cell Counter. Then, cells were partitioned into Gel Bead In Emulsions with a Target Cell Recovery of 10,000 total cells. Sequencing libraries were prepared using the v3.0 single-cell 3' mRNA kit (10x Genomics, Pleasanton, CA) with some adaptations for cell hashing, as indicated in TotalSeq™-A Antibodies and Cell Hashing with 10x Single Cell 3' Reagent Kit v3 Protocol from BioLegend. Briefly, 1 µl of 0.2 µM hashtag oligonucleotide (HTO) primer (GTGACTGGAGTTCAGACGTGTGC*T*C; *phosphorothioate bond) was added to the cDNA amplification reaction to amplify the hashtag oligos together with the full-length cDNAs. A SPRI selection clean-up was performed to separate mRNA-derived cDNA (>300 bp) from antibody-oligo-derived cDNA (<180 bp), as described in the above-mentioned protocol. 10x Genomics cDNA libraries were prepared following the 10x Genomics Single Cell 3' mRNA kit protocol, while HTO cDNAs were indexed by PCR as follows. Briefly, 5 µl of purified hashtag oligo cDNA were mixed with 2.5 µl of 10 µM Illumina TruSeq D70X_s primer (IDT) carrying a different i7 index for each sample, 2.5 µl of SI primer from 10x Genomics Single Cell 3' mRNA kit, 50 µl of 2xKAPA HiFi PCR Master Mix (KAPA Biosystem) and 40 µl of nuclease-free water. The reaction was carried out using the following thermal cycling

conditions: 98°C for 2 min (initial denaturation), 12 cycles of 98°C for 20 sec, 64°C for 30 sec, 72°C for 20 sec, and a final extension at 72°C for 5 min. The HTO libraries were purified with 1.2X SPRI bead selection. Size distribution and concentration of cDNA and HTO libraries were verified on an Agilent Bioanalyzer High Sensitivity chip (Agilent Technologies, Santa Clara, CA). Finally, sequencing of HTO and cDNA libraries was carried out on a NovaSeq6000 system (Illumina Inc., San Diego, CA) to obtain approximately >25,000 reads per cell.

Data processing of scRNA-seq.

To profile the cellular transcriptome, we processed the sequencing reads using the CellRanger software package (version 6.1.1) from 10X Genomics Inc. We mapped the reads against the human GRCh38 reference genome. For the libraries where multiple samples were pooled together, we also specified the HTO associated to each sample. All analyses presented in this manuscript were conducted using R version 4.0.5, along with specific analysis and data visualization packages such as Seurat R package (version 4.0.0) (*6*) SeuratObject package (version 4.0.1), and other packages specified in the subsequent sections. All plots were generated using ggplot2 package (version 3.3.3). For sample demultiplexing, we demultiplexed cell hashtags as described in Stoeckius et al. (*7*) for each library separately. Briefly, we normalized HTO counts using a centered log ratio and run "HTODemux()" function from Seurat package with the default parameters. Each barcode was classified to its sample-of-origin, and multiplets (barcodes assigned to more than one condition) or negatives (barcodes not assigned to any condition) were discarded for downstream analysis. For quality control (QC) and cell annotation, we ensured that there were no remarkable differences on the main QC metrics (library size, library complexity, percentage of mitochondrial and ribosomal expression) among the different hashed and non-hashed libraries, and then performed common QC, normalization and further analysis following the guidelines provided by Leucken et al. (*8)*.

We removed low-quality cells by filtering out barcodes with a very low number of Unique Molecular Identifiers (UMIs) (500) and genes (<250), or with a high percentage of mitochondrial expression (>20%), as it is indicative of lysed cells. Additionally, we considered removing barcodes with a large library size (>50,000) and complexity (>6,000) as they could be putative doublets. We eliminated genes that were detected in very few cells (<10). Finally, filtered data were normalized, log transformed and shared 3,000 highly variable features were used to compute Principal Component Analysis. To achieve successful cell-type annotation combining data from different donors and treatments, we removed the batch-effect with the Harmony integration method (*9*) using the library as a confounder variable. After integration, we created a k-nearest neighbors graph with the "FindNeighbors" function using the first 20 Principal Components, followed by the cell clustering with the Louvain clustering algorithm using the "FindClusters" function at different resolutions. To visualize scRNA-seq data in two-dimensional embedding, we run the Uniform Manifold Approximation and Projection algorithm. To obtain a fine-grained cell type annotation, we followed a top-down approach; first, cells were clustered into large clusters representing cell lineages (B lymphocytes, myeloid cells, T lymphocytes and NK cells), subsequently, cells from the lineages of interest were re-processed and clustered, or even sub-clustered, to define cell types and cell states. To annotate the clusters into specific cell types, we performed a Differential Expression Analysis (DEA) for all clusters to determine their marker genes using the normalized RNA counts, we examined the expression of canonical gene markers, and referred to gene markers from published annotated datasets. Low quality clusters based on poor QC metrics or platelet complexes showing dual gene markers were removed. We performed DEA for cell annotation using the Seurat function "FindMarkers" with the Wilcoxon signed-rank sum test. We defined genes to be relevant markers if the Log2 Fold Change (Log2FC) >0.25, with a FDR adjusted p-value <0.05, and if they were present in at least 25% of cells. For cell type compositional analysis and

to estimate changes in the proportions of cell types due to albumin treatment, we compared the fraction of cell types relative to all cells within each lineage population, and computed a paired Wilcoxon signed-rank sum test for each cell type comparing albumin with vehicle treated samples for AD patients and healthy donors, independently. To validate the albumin effect on CD4 T cells using scRNA-seq data, we downloaded the list of genes associated with the BTM of interest and computed a signature-specific score for each cell using the Ucell package (*10*). The BTM signature score was then assessed on specific cell populations across treatment conditions. Statistical analysis between albumin and vehicle treatment conditions was performed using a paired Wilcoxon signed-rank sum test. The code to reproduce the full analysis is hosted at Github: https://github.com/LJimenezGracia/AD-ACLF_cirrhosis_HSAtreatment.

Bulk whole blood RNA-seq.

RNA was isolated from blood stored in Tempus tubes using the Tempus™ Spin RNA Isolation Kit (Applied Biosystems, Foster City, CA) as previously described (*5*). RNA quality was assessed using Agilent RNA 6000 Nano and Pico Chips (Agilent Technologies) and concentration via Qubit RNA HS Assay Kit (Thermo Fisher Scientific). Sequencing libraries were prepared using the TruSeq Stranded Total RNA with Ribo-Zero Globin kit and TruSeq RNA CD Index Plate (both from Illumina Inc.) following TruSeq Stranded Total RNA Sample Prep-guide (Part # 15031048 Rev. E). Starting from 500 ng of total RNA, rRNA and globin mRNA were depleted, and remaining RNA was purified, fragmented, and primed for cDNA synthesis. cDNA first strand was synthesized with SuperScript-II Reverse Transcriptase (Thermo Fisher Scientific, Waltham, MA) for 10 min at 25°C, 15 min at 42°C, 15 min at 70°C and pause at 4°C. cDNA second strand was synthesized with Illumina reagents at 16°C for 1 hour. Then, A-tailing and adaptor ligation were performed. Finally, enrichment of libraries was

achieved by PCR (30 s at 98°C; 15 cycles of 10 s at 98°C, 30 s at 60°C, 30 s at 72°C; 5 min at 72°C and pause at 4°C). Afterwards, libraries were visualized on an Agilent 2100 Bioanalyzer using Agilent High Sensitivity DNA kit (Agilent Technologies), quantified using Qubit dsDNA HS DNA Kit (Thermo Fisher Scientific) and sequenced in a NovaSeq-6000 (Illumina Inc.) by at least 100 million paired-end 100nt reads. The reads were aligned to the hg38 genome assembly and the transcriptome using STAR v2.5.3a6 and GENCODE 26 annotation (*11*). RNA-Seq by Expectation Maximization (RSEM) v1.3.0REF.8 was used to compute the expected read counts of each sample from the corresponding binary alignment map (known as BAM) files. Trimmed mean of M values normalization method and limma-voom transformation from rounded expected counts were used to normalize the nonbiological variability. Using the HUGO Genome Nomenclature Committee, which is a resource for approved human gene nomenclature, we included protein-coding genes, and among other gene locus types, immunoglobulin genes, and T-cell receptor genes, resulting in a total of 14,520 genes for analysis. Genes brought by sexual chromosomes and mitochondrial DNA were not included in the analysis. Differential expression between groups was assessed using the moderated t-statistic (*12*).

Data processing of bulk blood RNA-seq.

Bulk blood RNA-Seq data were used for different purposes, that are listed below. RNA-seq data have been deposited at the Gene Expression Omnibus (GEO accession number, GSE171741).

Assessing differential gene expression. DEGs were defined by the simultaneous presence of two criteria, i.e., an absolute FC greater than 1.5 and moderated P value of less than 0.05.

Analyzing gene-set enrichment. The QuSAGE method, as implemented in the QuSAGE package *(13)*, was used to conduct Gene Set Enrichment Analysis (GSEA) using the 346 blood

transcription modules (BTMs) as gene sets. BTMs are gene sets related to blood cells (e.g., plasma cells, immunoglobulins (M156.1)) developed through large-scale network integration of publicly available human blood transcriptomes (*14)*. QuSAGE provides an activity score for each gene set in each pairwise comparison. A BTM was identified as DE when the QuSAGE activity score of this BTM had a False Discovery Rate (FDR) <0.05 or P <0.05, where appropriate.

Analyzing shared genes and shared BTMs. A DEG or a differentially expressed BTM was defined as shared between two comparisons when the DEG or differentially expressed BTM were concordant in sign.

Assessing immune-cell signatures with the use of SingleR software. The SingleR software (*15)* was used to compare bulk blood RNA-seq data from our study participants with a reference dataset containing 114 human bulk RNA-seq samples of sorted immune-cell populations from 4 HS (GSE107011) *(16)*. This reference dataset contained 114 human RNA-seq samples annotated to 10 main immune-cell types, including neutrophils, basophils, monocytes, dendritic cells, T cells, CD4 T cells, CD8 T cells, progenitors, B cells, and NK cells. The GSE107011 dataset also contained samples that were additionally annotated to 29 fine immune-cell types, including low-density neutrophils, low-density basophils, classical monocytes, intermediate monocytes, nonclassical monocytes, plasmacytoid dendritic cells, myeloid dendritic cells, naïve CD8 T cells, central memory CD8 T cells, effector memory CD8 T cells, terminal effector CD8 T cells, naïve CD4 T cells, Th1 cells, Th1/Th17 cells, Th17 cells, Th2 cells, T regulatory cells, follicular helper T cells, terminal effector CD4 T cells, Vd2 gamma delta T cells, non-Vd2 gamma delta T cells, MAIT cells, progenitor cells, naïve B cells, non-switched memory B cells, switched memory B cells, exhausted B cells, plasmablasts, and NK cells. The SingleR pipeline compared our bulk blood RNA-seq data, first with the 10 main immune-cell types of reference and then with the 29-fine immune-cell types. In brief, the annotation in SingleR was performed

for each whole blood transcriptome independently. The first step was to identify variable genes among each reference immune-cell types. Variable genes were defined as the top N genes that had a higher median expression in a cell-type compared to each other cell-type; here we used 70 variable genes per cell-type for the first round of analysis. Using only variable genes increased the ability to distinguish closely related cell-types. Then, a Spearman coefficient was calculated for whole blood RNA expression with each of the samples in the reference dataset. The correlation analysis was performed only on variable genes in the reference dataset. Next, multiple correlation coefficients per sample according to the named annotations of the reference dataset were aggregated to provide a single value per cell-type per sample. Of note, SingleR uses the 80^{th} percentile of correlation values, to prevent misclassification due to heterogeneity in the reference samples. Finally, in the fine-tuning step, SingleR reran the correlation analysis, but only for the top cell-types from the previous step. The lowest value cell-type was removed (or values more than 0.05 below the top value), and then this step was repeated until only two cell-types remained. The cell-type corresponding to the top value after the last run was assigned to the blood sample.

Bulk RNA-seq and real-time PCR in PBMCs

Isolation of total RNA from PBMCs was performed using the TRIzol reagent following the manufacturer's instructions. RNA concentrations were assessed in Microvolume UV-Vis Spectrophotometer (Nanodrop One, Thermo Fisher Scientific). Bulk RNA-seq was performed as described above. For real-time PCR analysis, cDNA synthesis from 500 ng of total RNA was performed using the High-Capacity cDNA Archive Kit (Applied Biosystems, Foster City, CA). Real-time PCR analysis of human IGHA1 (Hs00733892_m1, encoding IgA1), IGHM (Hs00941538_g1, encoding IgM) and IHG2 (Hs00390545_3, customized, encoding IgG2) was

performed in QuantStudio™ 7 Pro Real-Time PCR System (Thermo Fisher Scientific) using RPS18 (Hs01375212_g1, encoding for RPS18) as endogenous control.

Neutrophil degranulation assay.

After 30 minutes of resting, neutrophils were seeded at a density of $3x10^6$ cells/mL and incubated with either HSA, recombinant human albumin (both at 15 mg/ml) or vehicle control in the absence or presence of phorbol 12-myristate 13-acetate (100 nM) for 2 hours at 37ºC in a 5% CO_2 incubator. At the end of the incubation period, supernatants were collected to measure degranulation using the Neutrophil MPO Activity Assay Kit (Cayman Chemical, Ann Arbor, MI). Briefly, 25 µl of neutrophil supernatant together with 25 µl of assay buffer were added to each well of the experimental plate. Then, 50 µl of 3,3',5,5'-tetramethylbenzidine (TMB), a substrate for horseradish peroxidase, were added to each well and absorbance was measured at minute one and minute five after the addition of TMB in a microplate reader (Infinite M PLEX Monochromator, TECAN, Männedorf, Switzerland). The assay was performed at room temperature.

Neutrophil phagocytosis assay.

After 30 minutes of resting, neutrophils were seeded at a density of $5x10^5$ cells/mL and incubated with either HSA, recombinant human albumin (both at 15 mg/ml) or vehicle control for 2 hours at 37ºC in a 5% CO_2 incubator. Thereafter, 50 µL of opsonized fluorescein conjugate zymosan bioparticles or fluorescent-labeled *E. coli* (Thermo Fisher Scientific) were added to each well (ratio cells/bioparticles, 1:10) to a final volume of 200 µL and incubated at 37ºC for 60 min. Cells were then washed with sterile $DPBS^{--}$ and 100 µL trypan blue solution (diluted 1/10 in sterile $DPBS^{--}$) were added to quench fluorescence of extracellular bioparticles. Plates were finally centrifuged for 5 min at 400 g at room temperature and excess trypan blue was

carefully aspirated. The fluorescent intensity of each well was read in a microplate reader (FLUOstar Optima, Ortenberg, Germany).

Neutrophil chemotaxis assay.

A chemotaxis-phagocytosis assay in microfluidic arenas (*17*) was used to test the role of albumin on the ability of neutrophils to migrate directionally towards and to phagocytose *Candida albicans* yeast. For this purpose, microfluidic arenas were fabricated in PDMS and glass at the BioMEMS Core. The arenas were primed with a suspension of *Candida* yeast at 107 yeast cells/ml. The channels outside the arenas were washed with media to remove any extra *Candida* outside the arenas. After the addition of neutrophils to the chemotaxis assay in the presence or absence of HSA, images of the arenas were recorded on a Nikon Ti-E microscope with a motorized stage and environmental chamber. The number of neutrophils recruited to each arena was counted form brightfield images over time. The total area of GFP-expressing *Candida* was quantified from fluorescence images.

Swarming assay.

A swarming assay was used to test the contribution of HSA to the ability of neutrophils from patients to contain the growth of *Candida* clusters. To this purpose, arrays of *Candida*-adherent spots (200 μm diameter) were printed utilizing a microarray printing platform (Picospotter PolyPico, Galway, Ireland) and a solution of poly-l-lysine (Sigma-Aldrich). The arrays were printed onto ultra-clean glass slides (Thermo Fisher Scientific). The printed slides were mounted into 16-well ProPlate wells (Grace Bio-labs, Bend, OR) and 50 μL of a suspension of *Candida* inoculums in PBS were added to each well and incubated with rocking for 5 min. Following incubation, the wells were washed with PBS to remove unbound yeast from the glass surface. The mounted slides were checked to ensure appropriate patterning of targets onto the

spots with minimal non-specific binding before use. Isolated neutrophils were counted and re-suspended in IMDM + 20% FBS with the indicated concentration of albumin or vehicle, and then added to swarming chambers at 500,000 cells per well. Swarming was observed using a Nikon Ti-E microscope. Time-lapse imaging was conducted using a 10x Plan Fluor Ph1 DLL (NA=0.3) lens and endpoint images were taken with a 2x Plan Apo (NA=0.10) lens. All selected points were optimized for perfect focus before launching the experiment. Fungal growth area analysis was automated in ImageJ software.

Supplementary figures

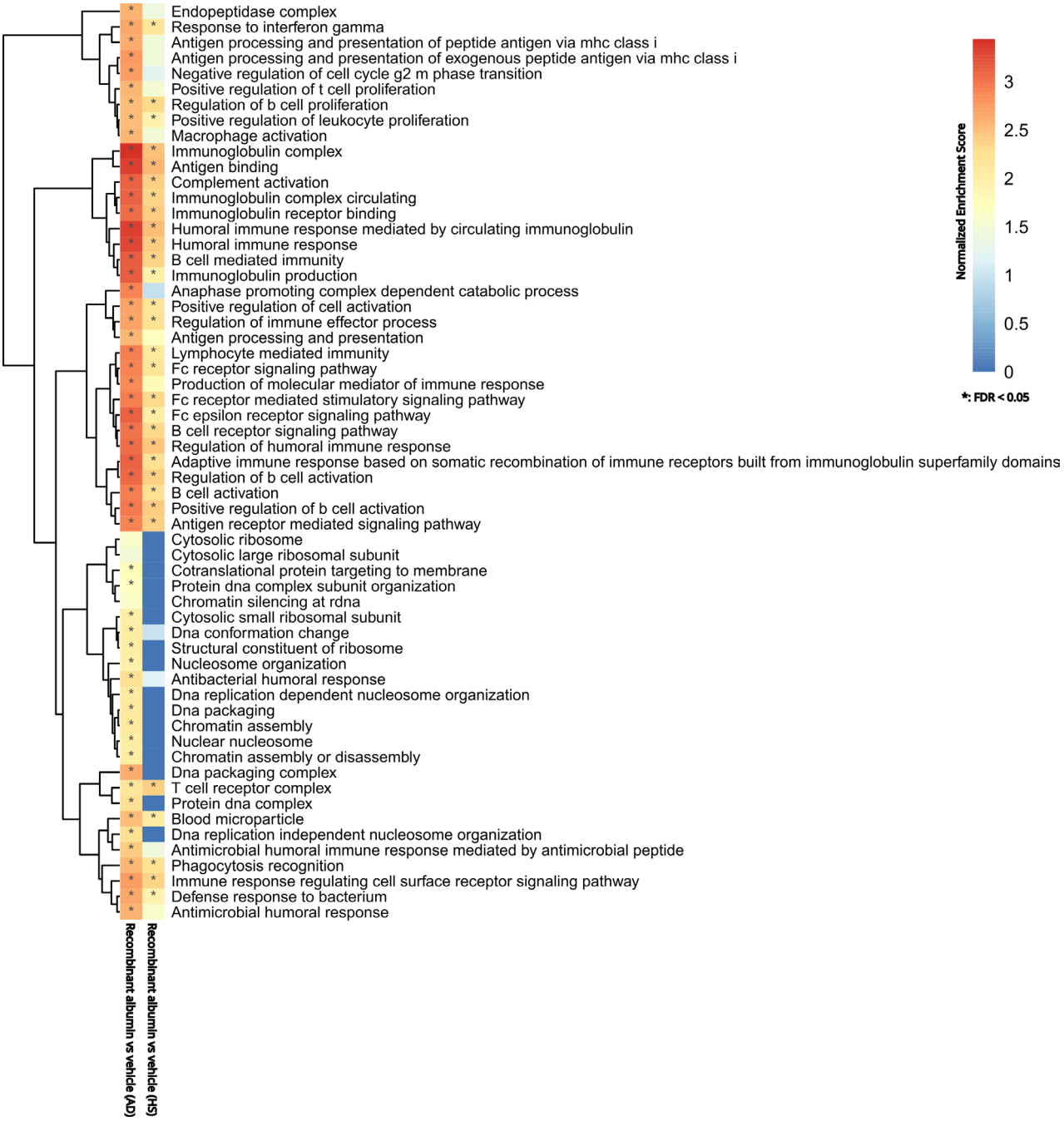

Fig. S1. **Changes in the transcriptional landscape of PBMCs isolated from HS incubated in vitro with recombinant albumin.** RNA-seq data were submitted to GSEA to generate ranked lists of genes for the following pairwise comparisons: recombinant albumin versus vehicle in PBMCs from patients with AD cirrhosis and recombinant albumin versus vehicle in PBMCs from healthy subjects. Gene-enrichment analysis was then performed. Color gradient corresponds to increasing values of the normalized enrichment score (NES) of gene sets from the less upregulated (in blue) to the most upregulated (in red). The presence of stars in cells of the heat map indicates a false discovery rate (FDR) <0.05. For comparison, the transcriptional changes in PBMCs isolated from patients with AD cirrhosis incubated *in vitro* with recombinant albumin are shown.

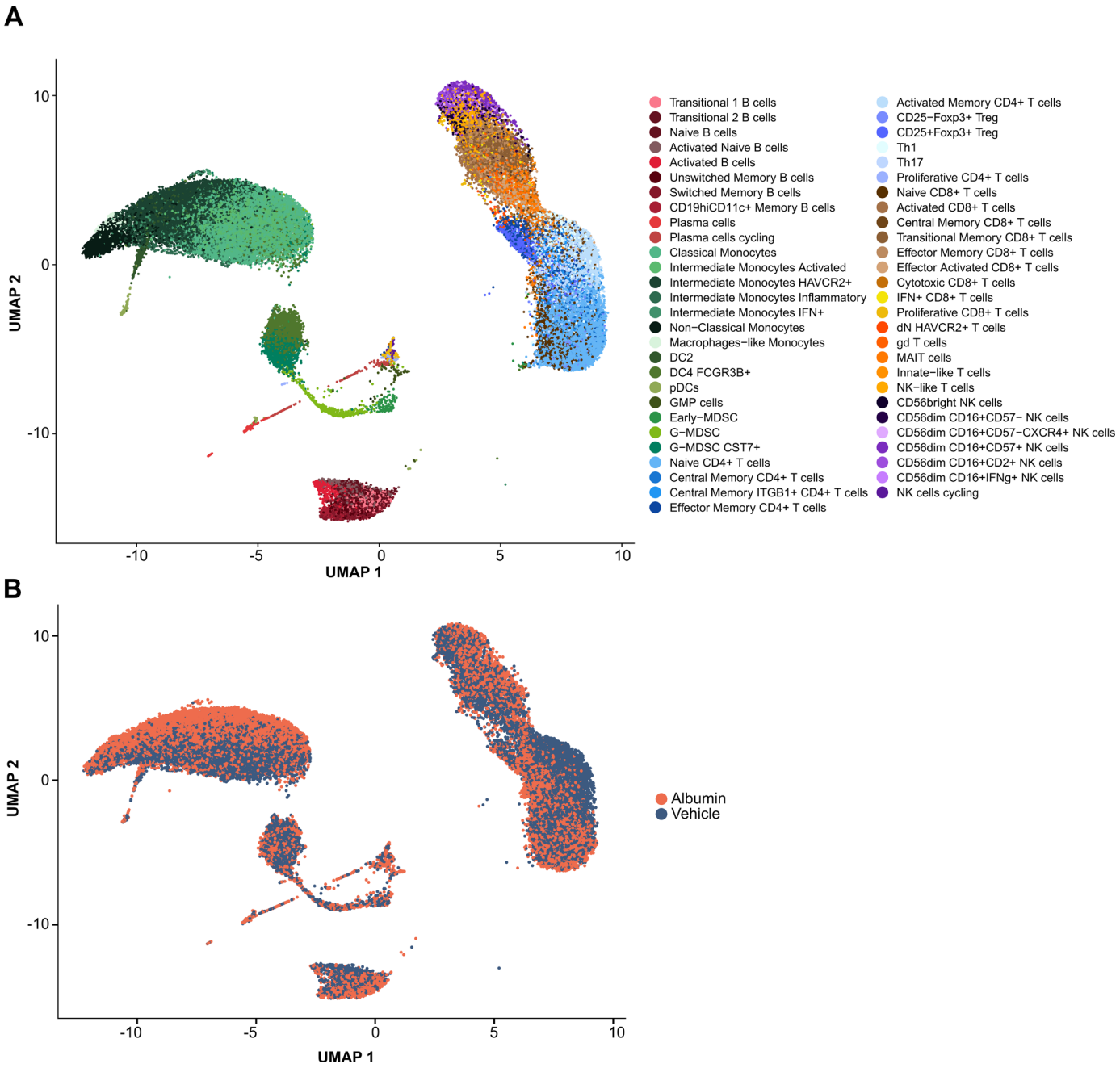

Fig. S2. Overview of results of scRNA-seq experiments of PBMCs from patients with AD cirrhosis. Fresh PBMCs from 9 patients with AD cirrhosis were exposed *in vitro* to albumin (15 mg/ml) or vehicle during two hours before performing scRNA-seq. (A) Uniform manifold approximation and projection (UMAP) of 69,293 human PBMCs from AD patients exposed to albumin and vehicle, colored by cell types (a total of 66,064 PBMCs were further analyzed after excluding NK cells). (B) Overlay of albumin and vehicle exposure on the full PBMC UMAP.

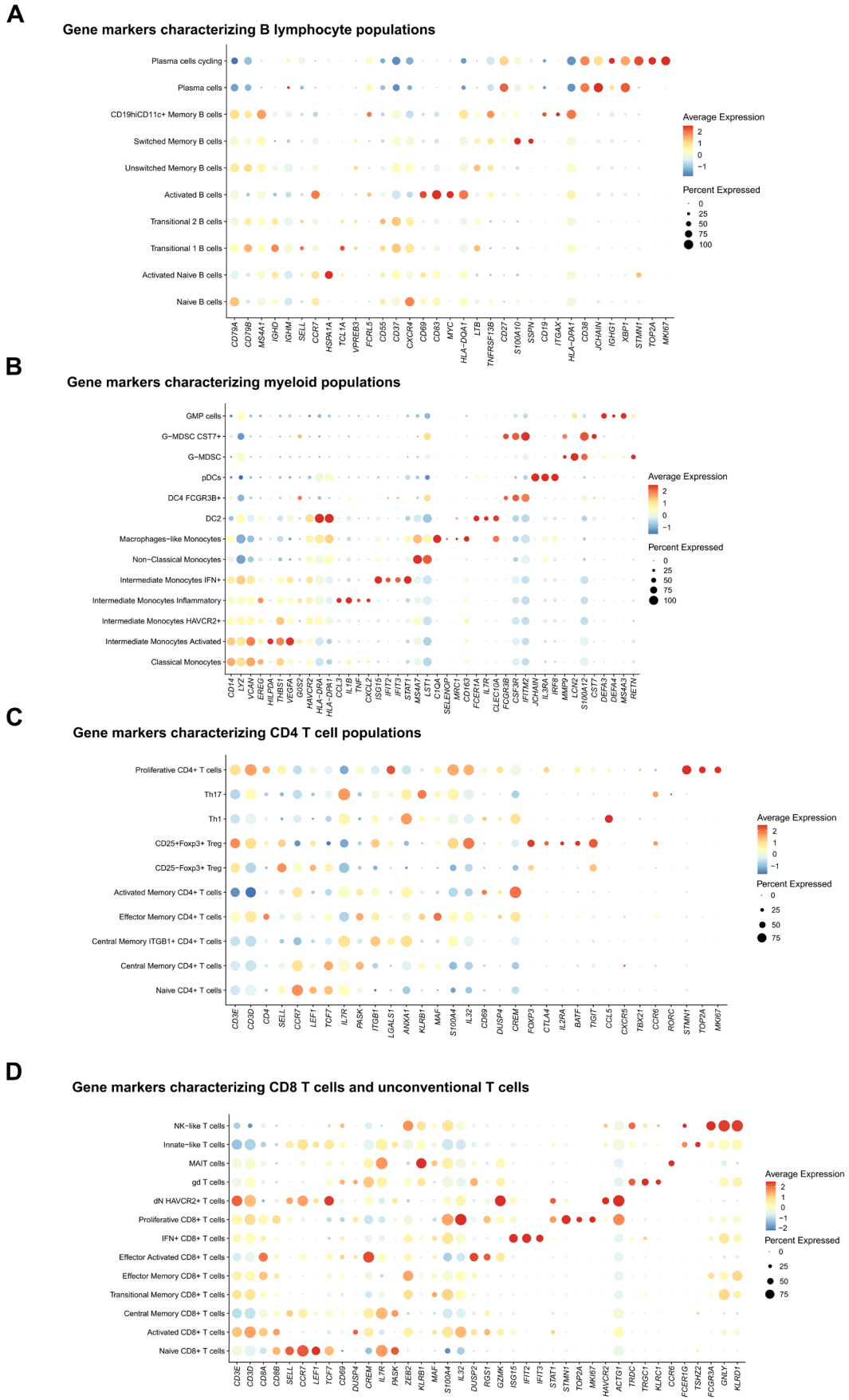

Fig. S3. Top gene markers describing all the immune-cell populations identified in the scRNA-seq dataset. Dot plot showing the average expression for top genes (*x-axis*) across all cell populations (*y-axis*) for B lymphocytes (A), myeloid cells (B), $CD4^+$ (C) and $CD8^+$ and unconventional T cells (D). Dot size represents the percentage of cells in a cluster expressing each gene, and the color indicates the average expression level.

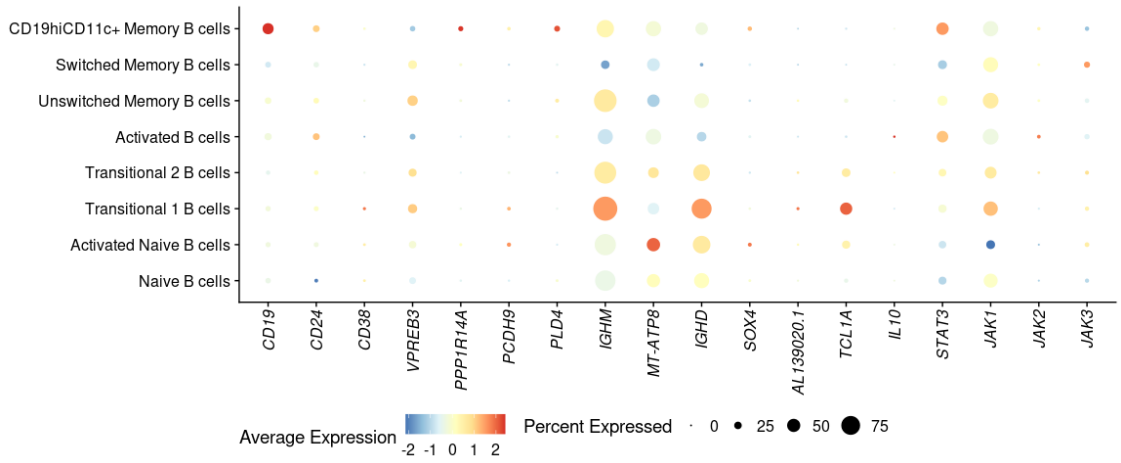

Fig. S4. Identity of the B cell populations affected by albumin using scRNA-seq data. Expression of genes associated with transitional-like identity from Steward et al. *(18)* across B cell populations, confirming that albumin induces transcriptional changes resembling transitional-like B cell signatures.

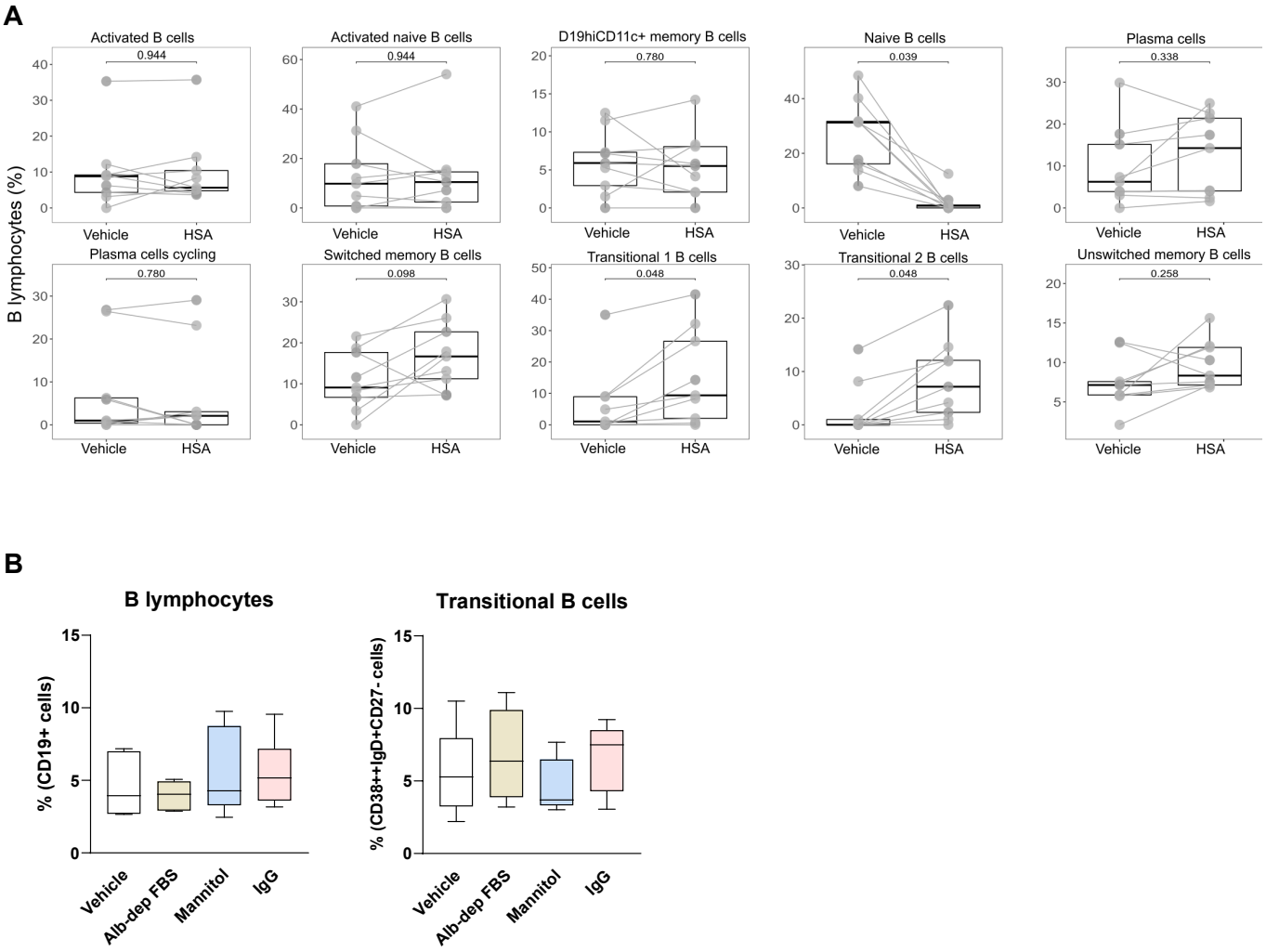

Fig. S5. In vitro effects of human serum albumin (HSA) on B lymphocytes. (A) Boxplots for the abundance of B lymphocyte populations using scRNA-seq data. All comparisons between HSA and vehicle were tested for significance with a paired Wilcoxon signed-rank sum test and adjusted p-values are indicated. This figure has been designed with results obtained in cells from 9 patients with AD cirrhosis. **(B)** Flow cytometry analysis of the B cell and transitional B cell populations in response to vehicle control, 15% albumin-depleted FBS (alb-dep FBS), mannitol (15 mg/ml) and IgG (15 mg/ml).

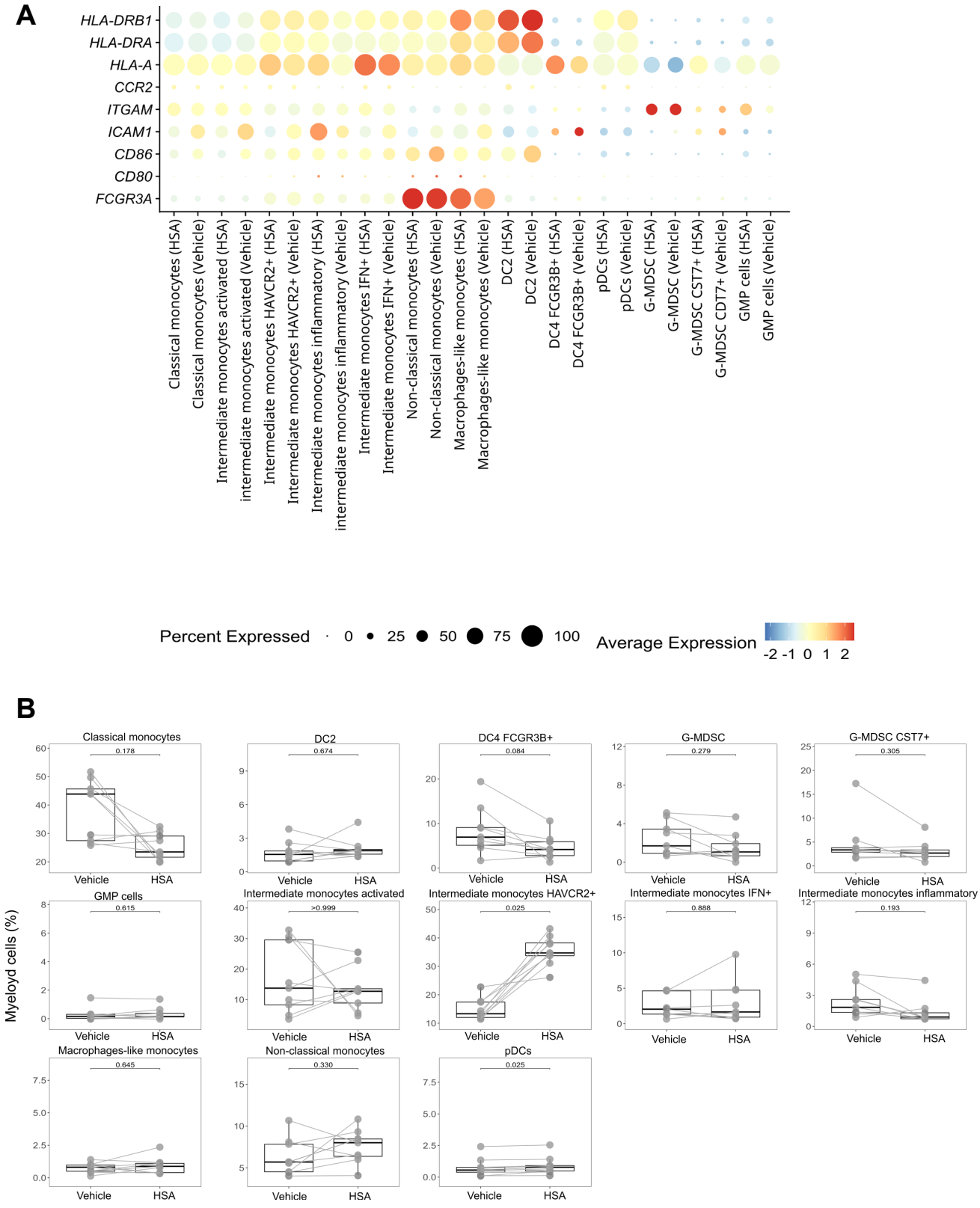

Fig. S6. Effects of HSA on myeloid cells using scRNA-seq. (A) Expression of genes associated with monocyte activation in cells exposed *in vitro* to either vehicle or HSA. **(B)** Boxplots for the abundance of myeloid cells. All comparison of cell type abundance between HSA and vehicle were tested for significance with a paired Wilcoxon signed-rank sum test, and adjusted p-values are indicated. This figure has been designed with results obtained in cells from 9 patients with AD cirrhosis.

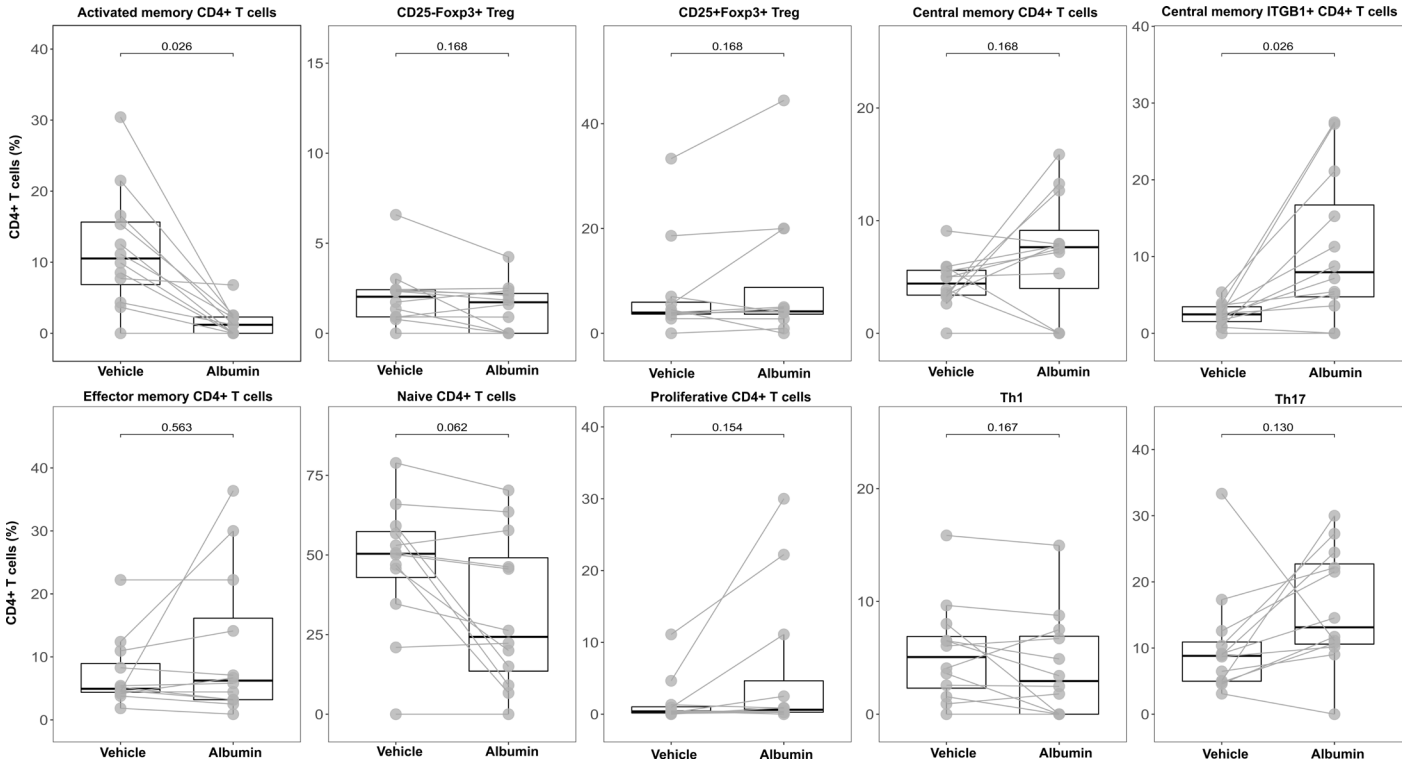

Fig. S7. Analysis of the cell type proportions for patients' CD4$^+$ T cells exposed *in vitro* to albumin. This figure has been designed with results obtained in cells from 9 patients with AD cirrhosis. Boxplots for the abundance of CD4$^+$ T cells. All comparison of cell type abundance between albumin and vehicle were tested for significance with a paired Wilcoxon signed-rank sum test; adjusted P values are indicated.

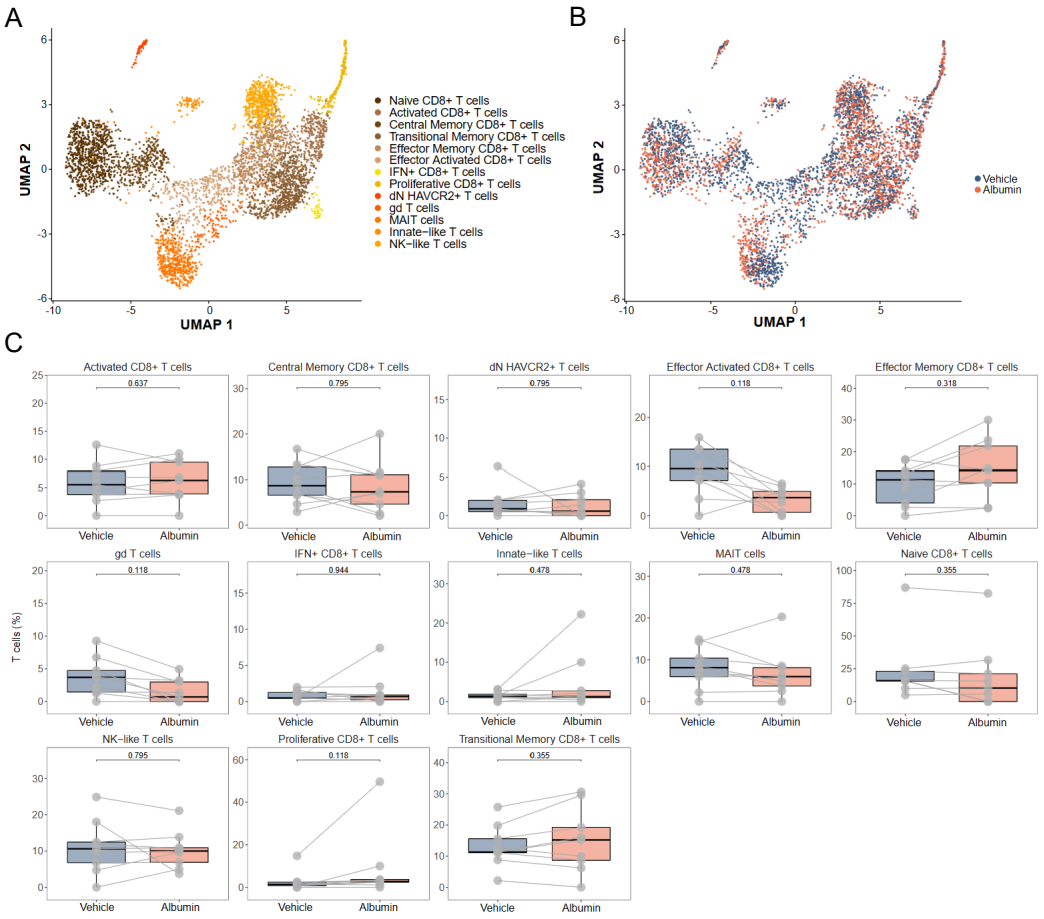

Fig. S8. Analysis of patients' CD8$^+$ and unconventional T cells exposed *in vitro* to albumin. This figure has been designed with results obtained in cells from 9 patients with AD cirrhosis. **(A)** UMAP of 3483 CD8$^+$ T cells and 1292 unconventional T cells exposed to albumin and vehicle, colored by cell populations. **(B)** Overlay of albumin and vehicle exposure on the CD8 and unconventional T-cell UMAP. **(C)** Box plots for the abundance of CD8 and unconventional T cell types after albumin exposure. All comparison of cell type abundance between albumin and vehicle were tested for significance using a paired Wilcoxon signed-rank sum test; adjusted p-values are indicated.

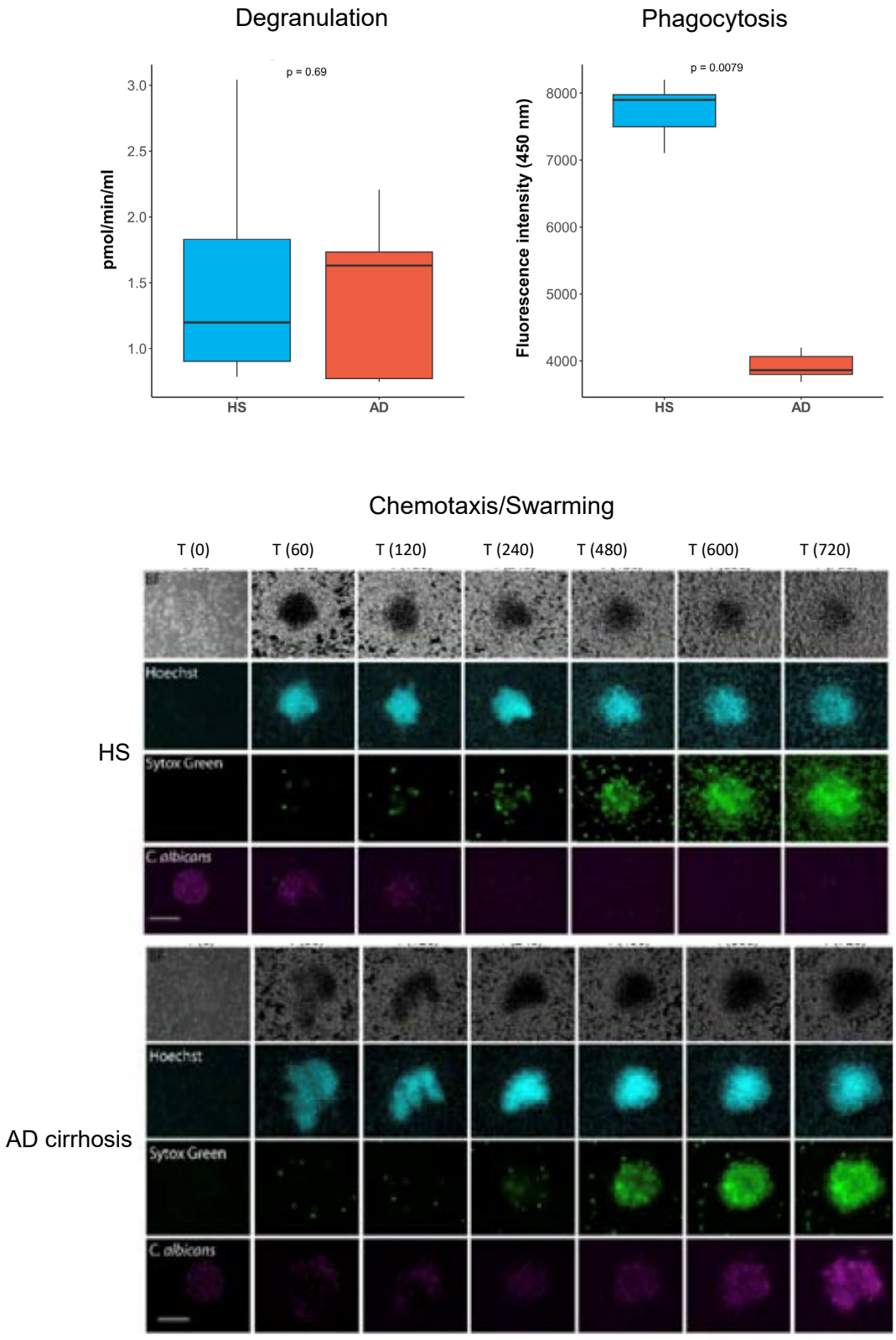

Fig. S9. Neutrophils from patients with AD cirrhosis exhibit impaired anti-microbial functions. Neutrophil degranulation was assessed by measuring the MPO enzymatic activity in the cell supernatants. Phagocytosis was assessed by ingestion of FITC-conjugated zymosan bioparticles. Chemotaxis and swarming were assessed through the ability of neutrophils to delay the escape of *Candida albicans* hyphae from the neutrophil swarm.

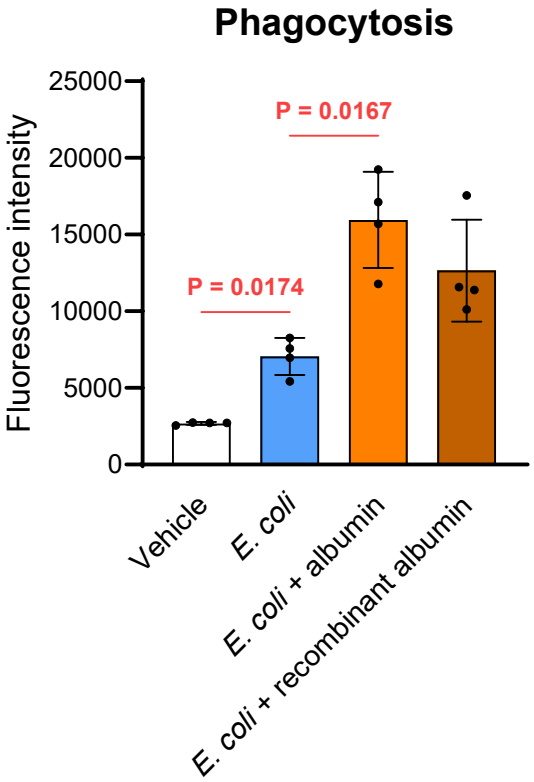

Fig. S10. Phagocytic capacity assessed by incubating neutrophils with fluorescently labeled *E. coli* alone or in the presence of albumin and recombinant albumin for 60 min and compared to vehicle control.

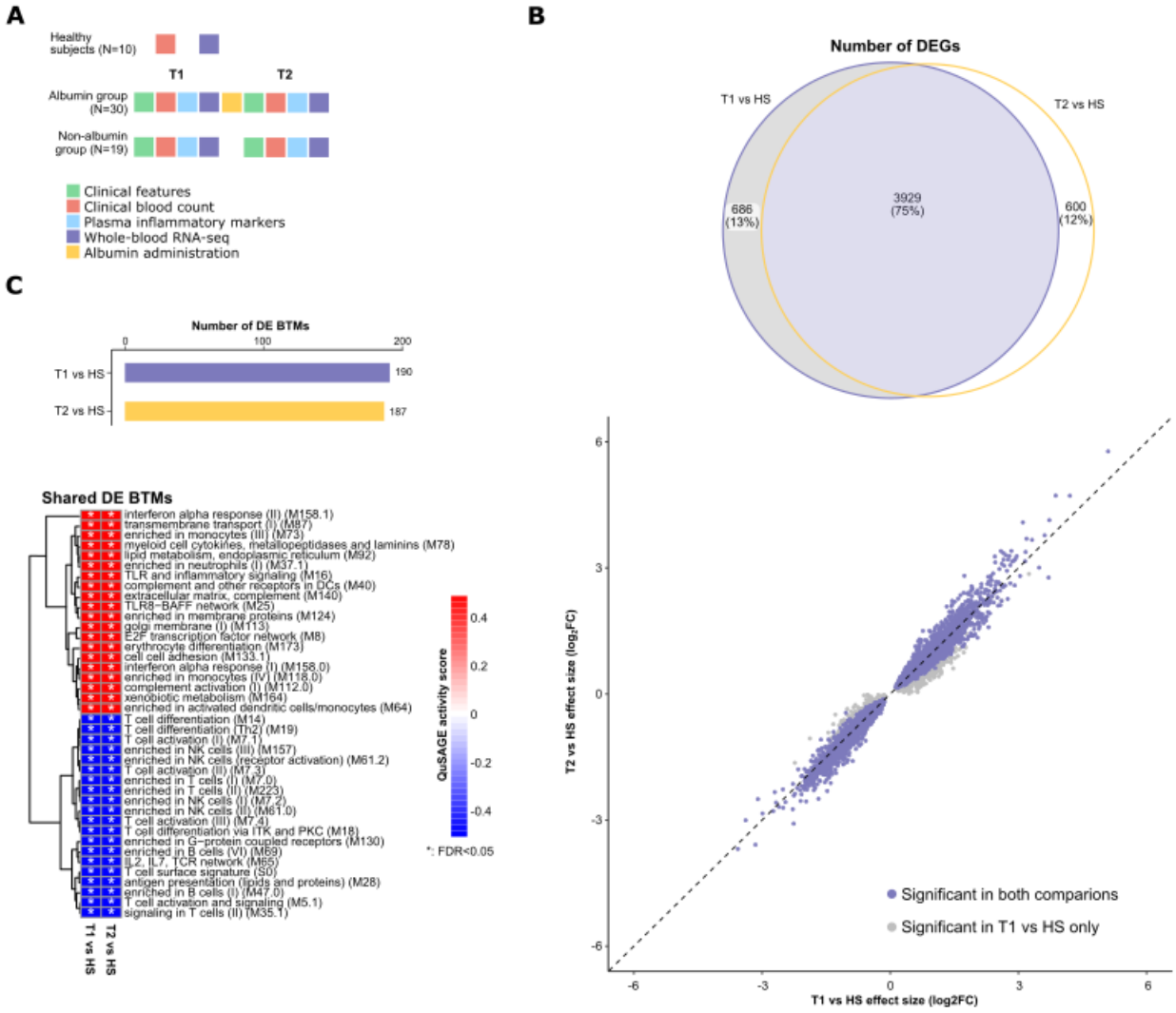

Fig. S11. Whole-blood transcriptional characteristics of all patients at T1 and T2 stages. **(A)** Overview of the longitudinal collection of clinical data and blood specimens (including blood that has been used for RNA-sequencing [RNA-seq]) in 49 patients at time 1 (T1, at enrollment) when they had AD cirrhosis and high risk of developing ACLF and at time 2 (T2) when they had progressed to ACLF. Thirty patients had received intravenous albumin when progressing from T1 to T2. Nineteen patients had not received albumin during the progression to ACLF. Ten age-matched healthy subjects were also studied, but only once. **(B)** Top, Venn diagram showing the overlap of differentially expressed genes (DEGs) in two pairwise comparisons, T1 vs healthy subjects and T2 vs healthy subjects. Bottom, Differential expression effect-size (log2 FC) of T2 compared with T1 changes for the 4615 T1 DEGs. **(C)** Top, number of differentially expressed (DE) blood transcription modules (BTMs) in two pairwise comparisons (T1 vs healthy subjects and T2 vs healthy subjects). Bottom, heatmap showing representative significantly upregulated BTMs and downregulated BTMs that are shared in two comparisons, T1 vs healthy subjects and T2 vs healthy subjects. BTMs are hierarchically clustered based on significant QuSAGE activity scores obtained in the comparison of T1 with healthy subjects. Asterisks denote false-discovery rate (FDR) <0.05. Color represents QuSAGE activity score.

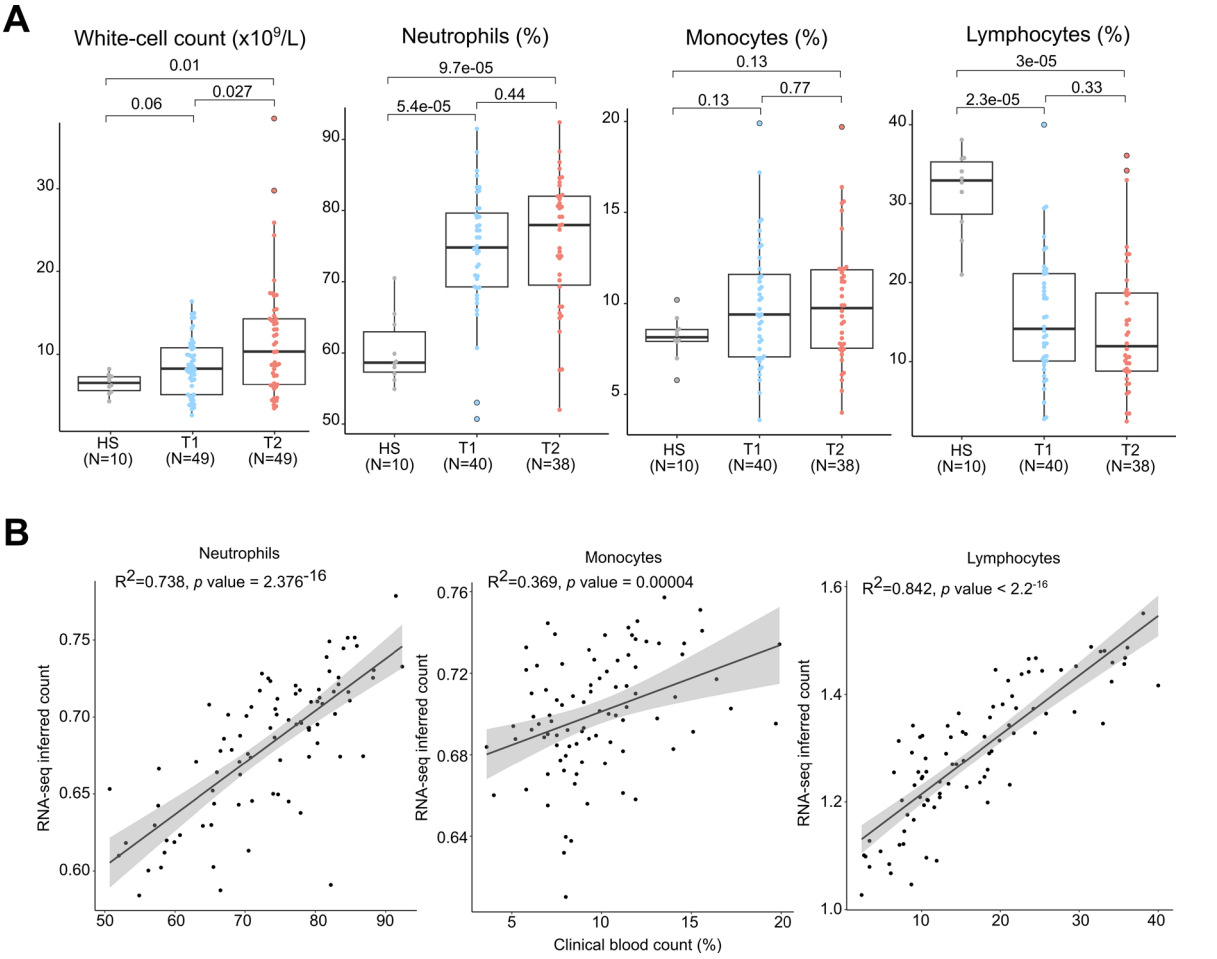

Fig. S12. Clinical blood counts and RNA-seq-inferred blood counts. Longitudinal collection of blood specimens was used for clinical blood count measurements and RNA-sequencing [RNA-seq]) in 49 patients at time 1 (T1, at enrollment) when they had pre-ACLF and at time 2 (T2) when they had progressed to ACLF. Ten age-matched healthy subjects were also studied, but only once. (A) Box plots of clinical complete blood counts were obtained in healthy subjects, and in patients at T1 and T2. There were no missing data in healthy subjects and for white blood cell count in patients. In patients, there were missing data for differential counts of neutrophils, monocytes, and lymphocytes in 2 patients. The horizontal line in each box represents the median, the lower and upper boundaries of the boxes the interquartile range, and the length of the vertical lines are 1.5 times the interquartile range. The P values are from Kruskal–Wallis tests followed by Mann–Whitney U tests. (B) Neutrophil, lymphocyte, and monocyte counts in paired clinical complete blood counts as compared with the RNA-seq-inferred blood counts obtained with the use of peripheral blood (47 paired specimens from healthy subjects, pre-ACLF and ACLF). The shaded areas represent the 95% confidence intervals. To obtain this figure, we correlated the clinical differential blood counts for neutrophils, monocytes and lymphocytes from all study participants including healthy subjects with the corresponding RNA-seq–inferred counts for these white cells (calculated based on the results of the SingleR software of RNA deconvolution for 10 main immune-cell types; see **Fig. S13A**).

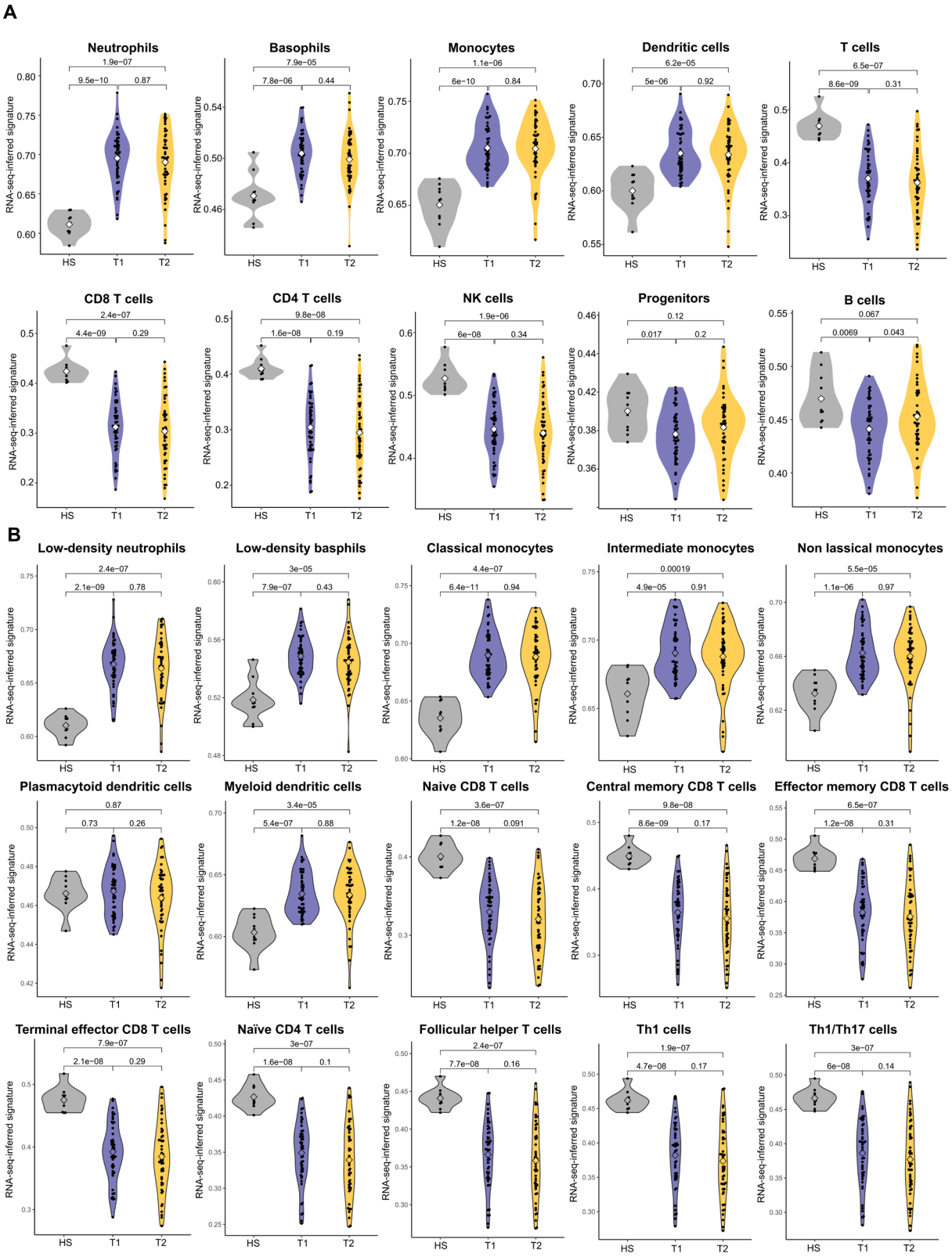

Continued on next page.

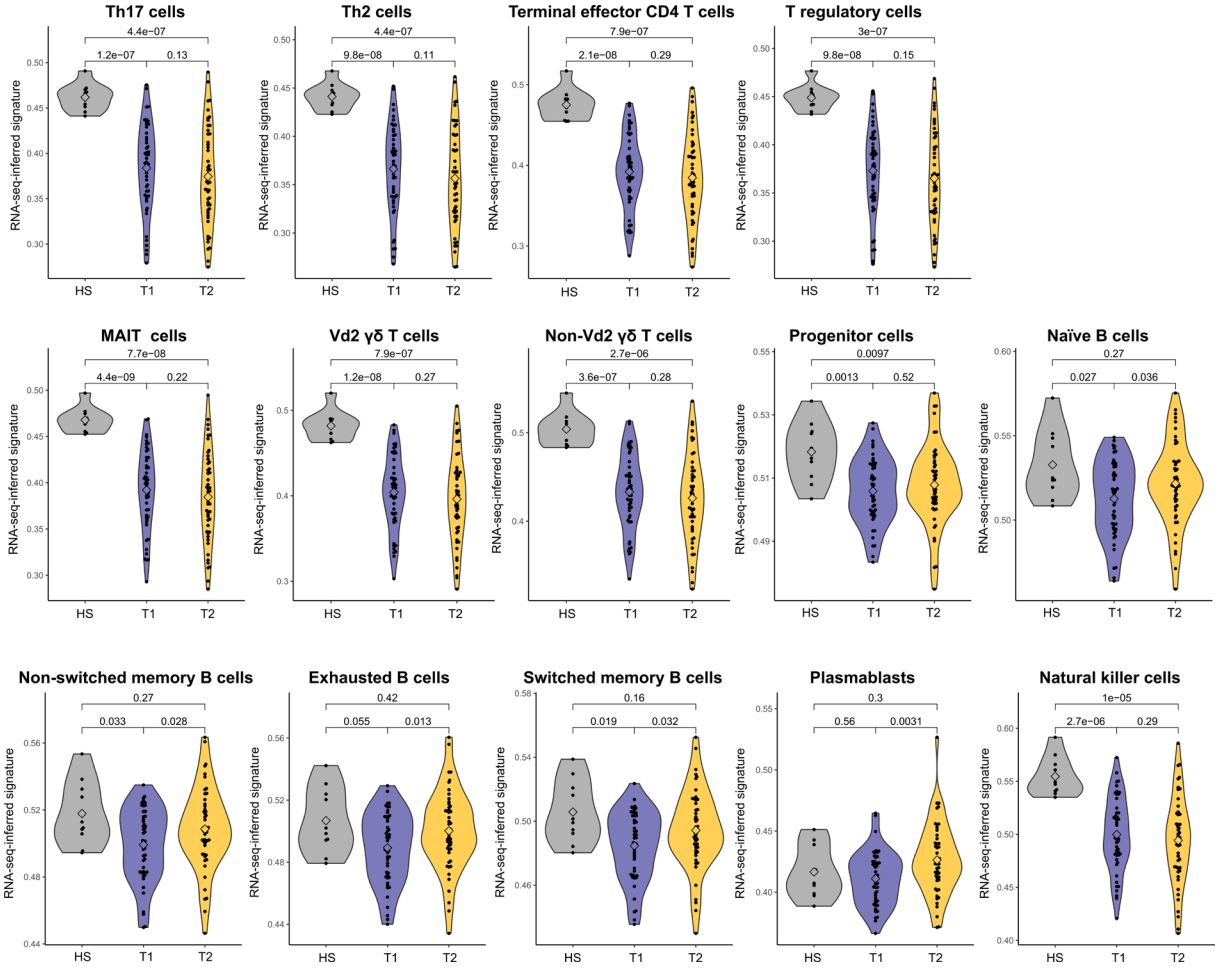

Fig. S13. Violin plots of RNA-seq-inferred signatures of blood immune cells in all patients at T1 and T2 and healthy subjects. Longitudinal collection of blood specimens was used for RNA-sequencing [RNA-seq]) in 49 patients, at time 1 (T1, at enrollment) when they had pre-ACLF, and at time 2 (T2) when they had progressed to ACLF. Ten age-matched healthy subjects were also studied, but only once. Whole-blood RNA-seq data were analyzed with the use of the SingleR software to determine signatures for each of the 10 main immune-cell types **(A)** and each of the 29-fine immune-cell types **(B).** White rhomboid symbols indicate medians. The P values are from Kruskal–Wallis tests followed by Mann–Whitney U tests.

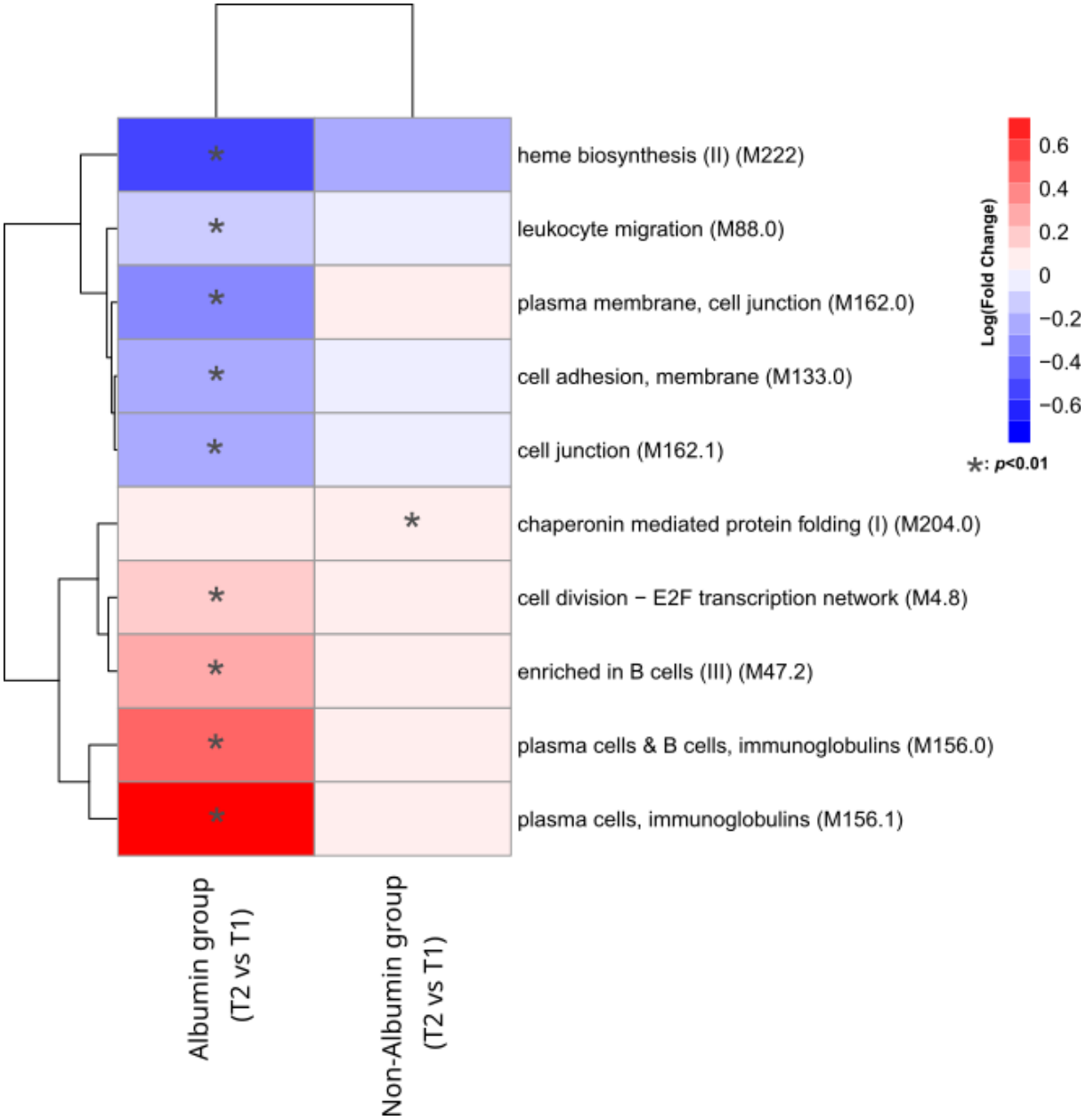

Fig. S14. Analysis of BTMs after adjusting by a non-linear regression multivariate model the transcriptomic data by disease severity of each patient estimated by the MELD score.

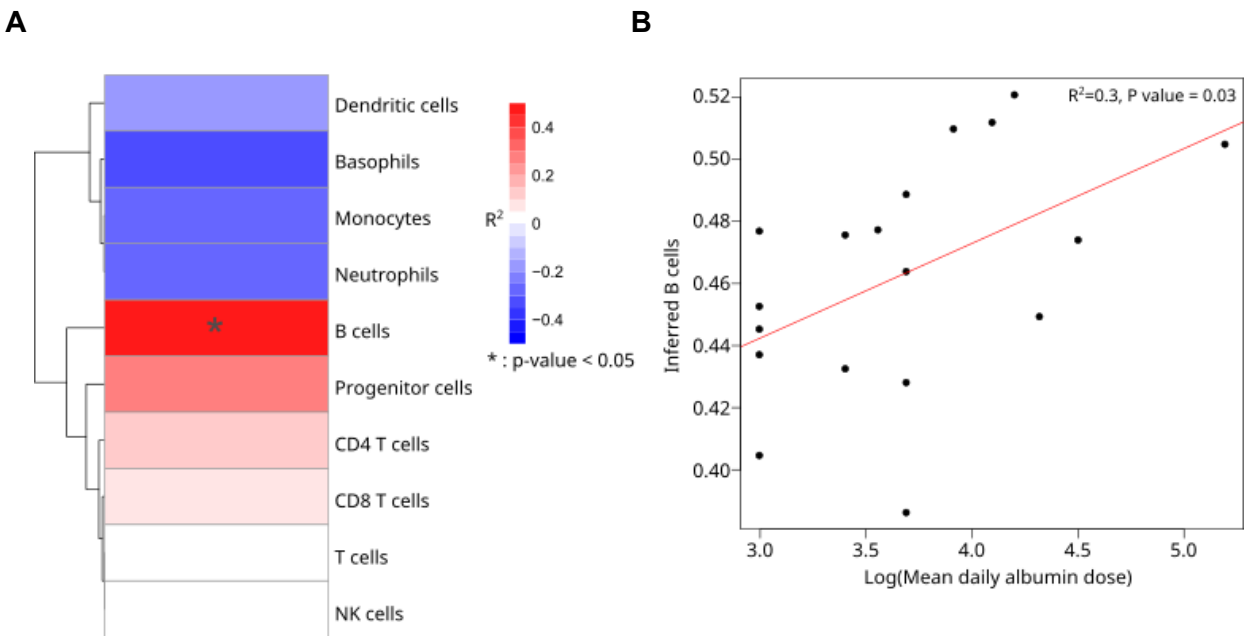

Fig. S15. (A) Correlation between mean daily albumin dose and the number of circulating immune cells inferred from Monaco cell population estimations. **(B)** Correlation between mean daily albumin dose and the number of B cells by means of Monaco estimation.

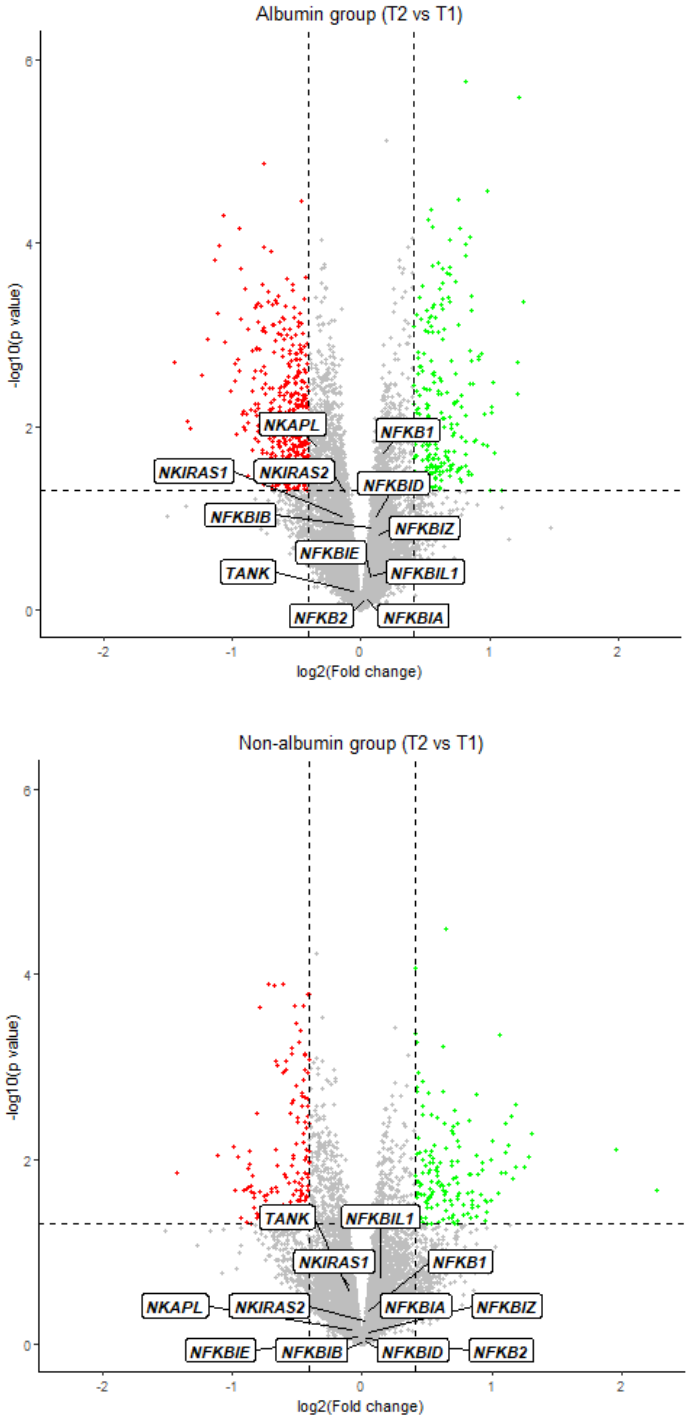

Fig. S16. Volcano plots showing differential expression effect-size (log2 FC) in genes of the NF-κB family between T2 and T1 plotted against significance (-log10 p value), for the albumin group (top) and non-albumin group (bottom). In both volcano plots, gray points indicate genes with no significant difference in expression between T2 and T1 (with absolute FC of less than 1.5 and P>0.05, i.e., -log10 P <1.3). *NFKB1,* Nuclear Factor Kappa B Subunit 1; *NFKB2,* Nuclear Factor Kappa B Subunit 2; *NKAPL*: NFKB Activating Protein Like, *NKAP,* NFKB Activating Protein; *TANK*, TRAF Family Member Associated NFKB Activator; *NKRF*, NFKB Repressing Factor; *NFKBIA*, NFKB Inhibitor Alpha; *NFKBIB*, NFKB Inhibitor Beta; *NFKBIZ*, NFKB Inhibitor Zeta; *NFKBID*, NFKB Inhibitor Delta; *NFKBIE*, NFKB Inhibitor Epsilon; *NFKBIL1*, NFKB Inhibitor Like 1; *NKIRAS1*, NFKB Inhibitor Interacting Ras Like 1; *NKIRAS2* ,NFKB Inhibitor Interacting Ras Like 2.

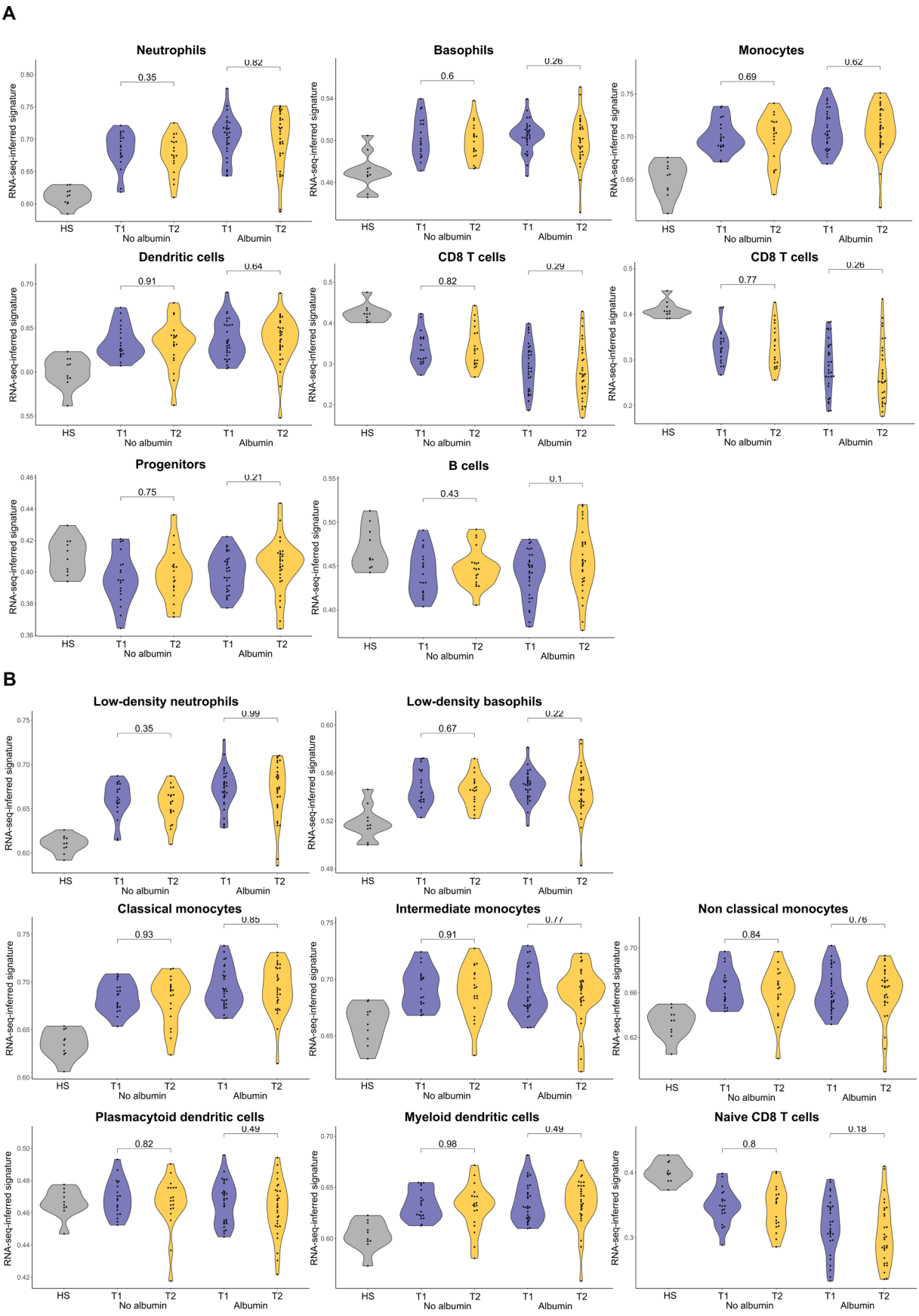

Continued on next page.

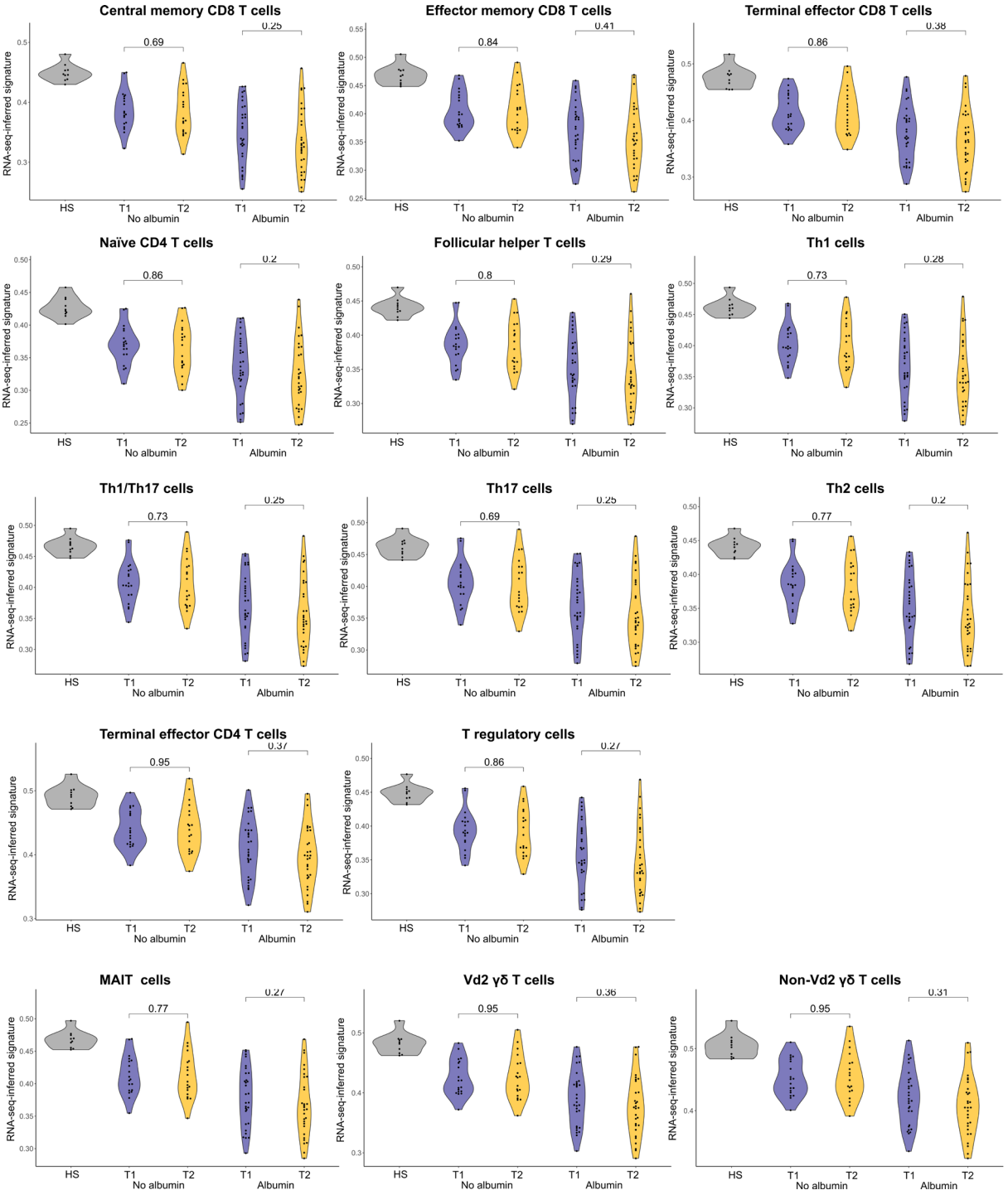

Continued on next page.

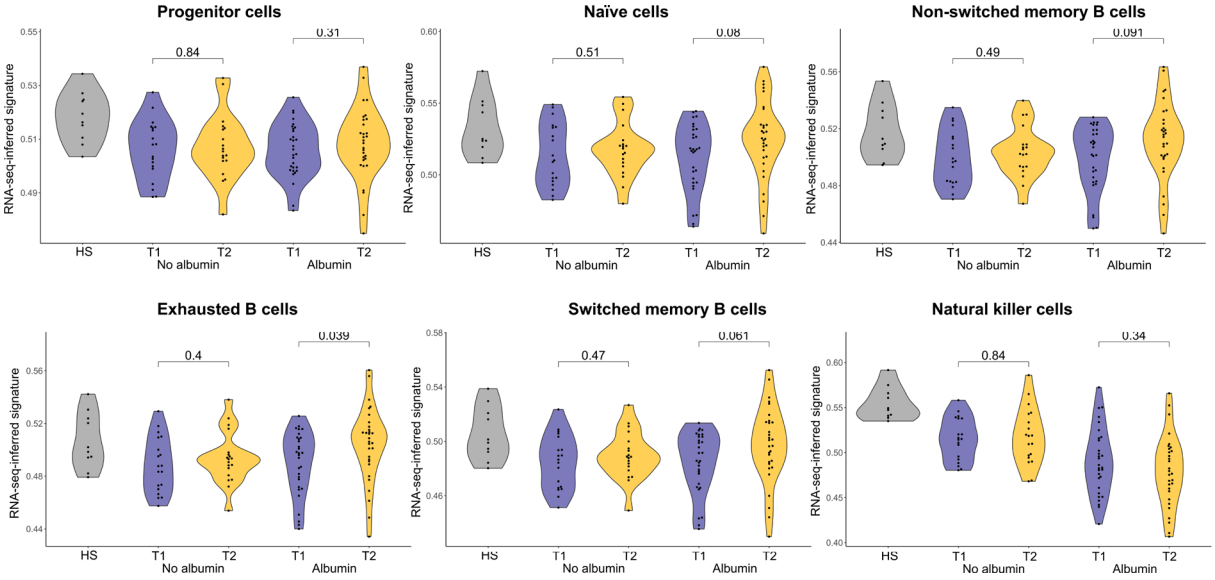

Fig. S17. Violin plots of RNA-seq-inferred signatures of blood immune cells at T1 and T2 in patients of the albumin group and those of the non-albumin group. Longitudinal collection of blood specimens was used for RNA-sequencing [RNA-seq]) in 49 patients at time 1 (T1, at enrollment) when they had pre-ACLF and at time 2 (T2) when they had progressed to ACLF. Thirty patients had received intravenous albumin when progressing from T1 to T2. Nineteen patients had not received albumin during the progression to ACLF. Whole-blood RNA-seq data were analyzed with the use of the SingleR software to determine signatures for each of the 10 main immune-cell types **(A)** and each of the 29-fine immune-cell types **(B).** Of note, results of plasmablasts are not shown in panel B because these results are shown in Figure 5D, top. Results obtained in 10 healthy subjects are provided for reference. The P values are from Kruskal–Wallis tests followed by Mann–Whitney U tests.

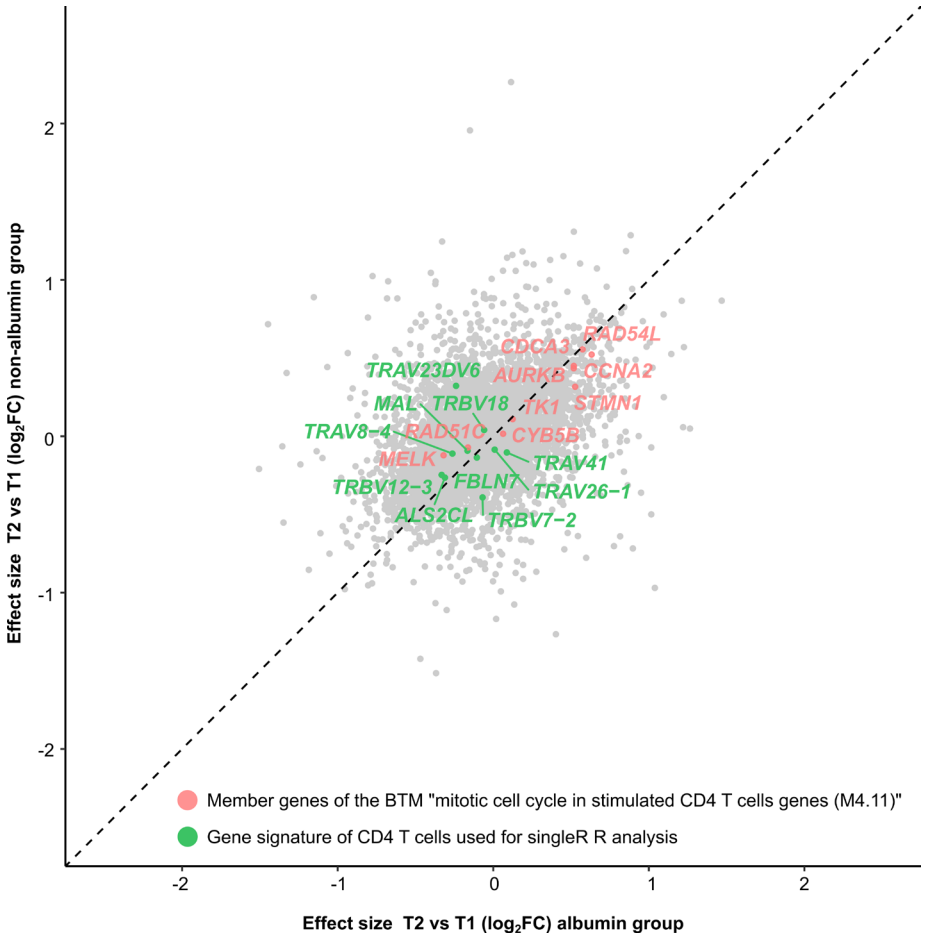

Fig. S18. Scatter plots showing the lack of overlap between member genes for the BTM related to mitotic cell cycle in stimulated CD4 T cells (M4.11) and genes defining the signature CD4 T cells used in the SingleR pipeline. There were 9 genes (red color) and 10 genes (green color), respectively.

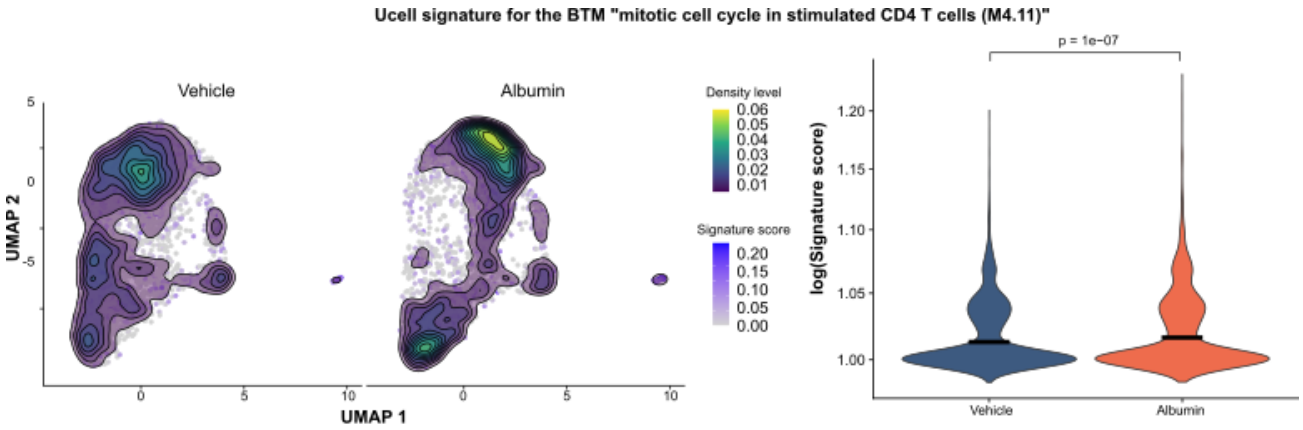

Fig. S19. Left, representative density plot showing the signature score for the BTM "mitotic cell cycle in stimulated CD4 T cells (M4.11)" on the CD4 T cells UMAP across vehicle and albumin conditions. Right, comparison of log(signature score) for the BTM 4.11 between albumin and vehicle on the CD4 T cell compartment. Statistical analysis for BTM signature was performed using a Wilcoxon signed-rank sum test; p-value significance is indicated. All comparison of cell type abundance between albumin and vehicle were tested for significance by paired Wilcoxon signed-rank sum test, and significant adjusted p-values are indicated.

Supplementary tables

Table S1. Characteristics of the thirty-four healthy volunteers and twenty patients with AD cirrhosis from whom PBMCs were isolated for *in vitro* experiments.

Characteristics	Healthy volunteers	Patients with AD cirrhosis
Demographic feature		
Age – yr	48.6±13.5	57.4±4.5
Male sex – no. (%)	17 (50)	15 (75)
Markers of organ function		
MELD score[†]	NA	22.3±8.8
CLIF-C OF score[‡]	NA	9±3.6
Organ system failure – no. (%)[§]	NA	
Liver failure	-	8 (40)
Kidney failure	-	6 (30)
Cerebral failure	-	3 (15)
Coagulation failure	-	7 (35)
Circulatory failure	-	12 (60)
Respiratory failure	-	0 (0)
ACLF grade – no. (%)	NA	
Grade 1	-	7 (35)
Grade 2-3	-	3 (15)
Precipitating events		
Infection – no. (%)	NA	6 (30)
Alcoholic hepatitis – no. (%)	NA	7 (35)
Laboratory data		
INR – median (IQR)	1.0 (0.9-1.0)	1.9 (1.5-2.4)*
Median total bilirubin (IQR) – mg/dL	0.6 (0.5-0.9)	4.9 (2-15.1)*
Median serum creatinine (IQR) – mg/dL	0.9 (0.7-1.0)	1.9 (1-2.3)*
Serum sodium – mmol/L	141.4±2.4	132.8±2.2*
Median serum albumin (IQR) – g/dL	4.6 (4.1-4.8)	2.8 (2.6-3.3)*
Median white-cell count (IQR) – $x10^3/mm^3$	6.4 (5.3-7.3)	6.6 (5.7-8.7)*
Median differential neutrophil count (IQR) – %	53.1 (46.0-60.5)	73 (65.0-79.0)*
Median differential lymphocyte count (IQR) – %	33.0 (28.4-41.8)	11 (5.4-19.2)*
Median differential monocyte count (IQR) – %	6.4 (5.4-7.8)	4.2 (0.2-7.7)*
Median blood C-reactive protein levels (IQR) – mg/L	0.1 (0.1-0.1)	3.2 (1.9-3.9)*

*Denotes statistical significance differences.

Plus–minus values are mean±SD.

MELD Model for End-Stage Liver Disease, CLIF-C Chronic Liver Failure Consortium, OF organ failure, INR International Normalized Ratio, IQR interquartile range.

Table S2. Characteristics of the nine healthy volunteers and six patients with AD cirrhosis from whom blood neutrophils were isolated for *in vitro* experiments.

Characteristics	Healthy volunteers	Patients with AD cirrhosis
Demographic feature		
Age – yr	49.9±10.7	61.3±9.9
Male sex – no. (%)	4 (55.6)	4 (66)
Markers of organ function		
MELD score†	NA	15.0±4.0
CLIF-C OF score‡	NA	5.3±0.8
Organ system failure – no. (%)§	NA	
Liver failure	-	0 (0)
Kidney failure	-	0 (0)
Cerebral failure	-	0 (0)
Coagulation failure	-	1 (17)
Circulatory failure	-	0 (0)
Respiratory failure	-	0 (0)
ACLF grade – no. (%)	NA	
Grade 1	-	0 (0)
Grade 2-3	-	0 (0)
Precipitating events		
Infection as pre-ACLF/ACLF precipitant – no. (%)	NA	0 (0)
Alcoholic hepatitis as pre-ACLF/ACLF precipitant – no. (%)	NA	0 (0)
Laboratory data		
INR – median (IQR)	1.0 (0.9-1.0)	1.3 (1.3-1.4)
Median total bilirubin (IQR) – mg/dL	0.8 (0.6-0.9)	1.9 (1.3-2.6)*
Median serum creatinine (IQR) – mg/dL	1.0 (0.9-1.1)	1.0 (0.8-1.2)
Serum sodium – mmol/L	141.6±1.3	134.8±4.2*
Median serum albumin (IQR) – g/dL	4.4 (4.2-4.6)	3.3 (2.8-3.6)*
Median white-cell count (IQR) – $x10^3/mm^3$	6.7 (4.0-7.0)	4.2 (3.1-5.4)
Median differential neutrophil count (IQR) – %	51.9 (45.3-62.1)	61.2 (56.5-71.8)*
Median differential lymphocyte count (IQR) – %	31.5 (26.4-44.6)	13.7 (6.0-23.9)*
Median differential monocyte count (IQR) – %	5.7 (5.0-6.6)	8.0 (2.5-9.6)
Median blood C-reactive protein levels (IQR) – mg/L	0.1 (0.1-0.1)	2.4 (1.8-3.0)*

*Denotes statistical significance differences.

Plus–minus values are mean±SD.

MELD Model for End-Stage Liver Disease, CLIF-C Chronic Liver Failure Consortium, OF organ failure, INR International Normalized Ratio, IQR interquartile range.

Table S3. Characteristics of the 49 Patients Enrolled in the HSA Infusion Study at T1 and T2 stages.

Characteristic*			P value
	T1	**T2**	
Age – yr	60.2±9.1[a]		
Male sex – no. (%)	33 (70)		
Markers of organ function			
MELD score	19.1±5.4	25.9±7.0	<0.01
CLIF-C OF score	7.1±1.1	9.9±2.4	<0.01
Organ system failure – no. (%)			
Liver failure	10 (20)	13 (27)	0.63
Kidney failure	0 (0)	36 (73)	<0.01
Circulatory failure	0 (0)	10 (20)	<0.01
Cerebral failure	1 (2)	7 (14)	0.07
Coagulation failure	0 (0)	8 (17)	0.01
Respiratory failure	0 (0)	9 (18)	0.01
ACLF grade – no. (%)			
Grade 1	0 (0)	27 (55)	<0.01
Grade 2-3	0 (0)	22 (45)	<0.01
Precipitating events			
Infection as precipitant at T1 or T2 – n (*%*)	17 (35)	24 (49)	0.22
Alcohol-related hepatitis as precipitant at T1 or T2 – n (*%*)	15 (31)	14 (29)	1
Laboratory data			
INR – median (IQR)	1.5 (1.2-1.7)	1.6 (1.4-2.1)	0.08
Median total bilirubin (IQR) – mg/L	3.5 (1.5-9.9)	3.9 (1.3-13.3)	0.86
Median serum creatinine (IQR) – mg/dL	1.3 (1.1-1.6)	2.3 (1.8-3.0)	<0.01
Serum sodium – mmol/L	132.4±6.3	133.0±-7.7	0.66
Median serum albumin (IQR) – g/dl	2.7 (2.3-3.3)	3.0 (2.6-3.4)	0.15
Median white-cell count (IQR) – $x10^3/mm^3$	7.7 (4.7-10.1)	9.7 (5.9-13.4)	0.03
Median absolute lymphocyte count (IQR) – $x10^3/mm^3$	1.0 (0.6-1.3)	1.1 (0.8-1.7)	0.19
Median absolute monocyte count (IQR) – $x10^3/mm^3$	0.7 (0.4-1.0)	0.9 (0.6-1.2)	0.13
Median absolute neutrophil count (IQR) – $x10^3/mm^3$	5.7 (3.5-7.4)	6.8 (3.9-10.3)	0.15
Median C-reactive protein (IQR) – *mg/L*	24.5 (11.2-42.8)	25.8 (13.4-65.8)	0.47
Median blood levels of protein mediators of inflammation (IQR) – pg/ml			
Eotaxin	70.2 (43.1-105.6)	80.2 (56.4-118.7)	0.19
G-CSF	20.1 (5.6-58.6)	21.7 (6.1-75.1)	0.84
Interferon-α2	11.3 (2.9-23.1)	16.8 (5.4-27.9)	0.30
Interferon-γ	26.2 (6.4-86.6)	25.2 (9.3-64.7)	0.81
Interleukin-1α	3.0 (1.3-5.7)	2.0 (0.7-4.7)	0.25
Interleukin-1β	5.4 (2.7-10.3)	5.2 (2.0-10.3)	0.93
Interleukin-6	17.0 (7.9-39.7)	27.1 (10.6-71.5)	0.07
Interleukin-8	4.9 (2.8-10.9)	5.8 (2.8-16.7)	0.57

Interleukin-10	6.1 (1.5-23.4)	5.8 (3.5-20.0)	0.43
IP-10 (CXCL10)	214 (131-376)	234 (148-540)	0.46
MIP-1α (CCL3)	11.4 (4.6-22.5)	14.1 (6.7-25.2)	0.28
MIP-1β (CCL4)	15.7 (11.8-20.7)	17.0 (12.7-28.7)	0.27
Tumor necrosis factor α	32.4 (17.9-43.6)	35.4 (21.8-60.3)	0.44
VEGF	4.4 (1.0-9.5)	7.6 (2.9-14.2)	0.09
Deaths – n (%)			
By 28 days	9 (18)		
By 90 days	23 (47)		

*Plus–minus values are mean±SD.

To convert the values for serum creatinine to micromoles per liter, multiply by 88.4. To convert the values for bilirubin to micromoles per liter, multiply by 17.1. Normal values for blood inflammatory mediators are shown in **Table S4**. MELD Model for End-Stage Liver Disease, CLIF-C Chronic Liver Failure Consortium, OF organ failure, INR International Normalized Ratio, IQR interquartile range, G-CSF granulocyte-colony stimulating factor, IP-10 interferon-inducible protein 10, CXCL C-X-C motif chemokine ligand, MCP-1 monocyte chemoattractant protein 1, CCL CC motif chemokine ligand, MIP macrophage inflammatory protein, and VEGF vascular endothelial growth factor.

Table S4. Plasma Levels (pg/ml) of Inflammatory Mediators in 78 Healthy Subjects.

Mediator	Median value (IQR)*
Eotaxin	41.2 (31.7-56.1)
G-CSF	5.6 (2.7-8.2)
IFN-α2	19.1 (10.8-37.2)
IFN-γ	15.2 (6.2-24.3)
Interleukin-1α	1.8 (0.7-4.7)
Interleukin-1β	2.6 (1.2-6.3)
Interleukin-6	0.4 (0.2-0.7)
Interleukin-8	0.3 (0.2-0.6)
Interleukin-10	2 (0.8-3.8)
IP-10 (CXCL10)	74.4 (55.3-103)
MIP-1α (CCL3)	7.6 (3.4-13.8)
MIP-1β (CCL4)	8.1 (6.5-10.1)
Tumor necrosis factor α	8.8 (6.1-14.5)
VEGF	6.3 (2.5-16.2)

*IQR denotes interquartile range, G-CSF granulocyte-colony stimulating factor, IP-10 interferon-inducible protein 10, CXCL C-X-C motif chemokine ligand, MCP-1 monocyte chemoattractant protein 1, CCL CC motif chemokine ligand, MIP macrophage inflammatory protein, and VEGF vascular endothelial growth factor.

Table S5 is provided as a separate .xls file. This table shows the results of enrichment analyses of the blood transcription module (BTM) space with the use of QuSAGE.

Supplementary video legend

The dynamics of neutrophil recruitment and candida growth. *Top left:* *Candida* only in microfluidic chambers. *Top right:* Neutrophils only in microfluidic chambers in the presence of LTB_4 (100 nM). *Bottom left:* Neutrophils recruited in the presence of albumin are more likely to swarm and contain any *Candida* growing in hyphae after phagocytosis. Neutrophil swarming appears to be attracting more neutrophils from outside the chambers. *Bottom right:* Neutrophils recruited in vehicle-control conditions phagocytose the yeast but are less likely to control the growth of *Candida* that escape the initial control and grown into hyphae. Fewer neutrophils are recruited after the neutrophils encounter *Candida* hyphae.

Supplementary references

1. Trebicka J, Fernandez J, Papp M, et al. The PREDICT study uncovers three clinical courses of acutely decompensated cirrhosis that have distinct pathophysiology. J Hepatol 2020;73:842-54.
2. Moreau R, Jalan R, Ginès P, et al. Acute-on-chronic liver failure is a distinct syndrome that develops in patients with acute decompensation of cirrhosis. Gastroenterology 2013;144:1426-37.
3. Arroyo V, Moreau R, Jalan R. Acute-on-Chronic Liver Failure. N Engl J Med 2020;382:2137-45.
4. Clària J, Stauber RE, Coenraad MJ, et al. Systemic inflammation in decompensated cirrhosis: characterization and role in acute-on-chronic liver failure. Hepatology 2016;64:1249-64.
5. Weiss E, de la Grange P, Defaye M, et al. Characterization of Blood Immune Cells in Patients With Decompensated Cirrhosis Including ACLF. Front Immunol 2021;11:619039.
6. Hao Y, Hao S, Andersen-Nissen E, et al. Integrated analysis of multimodal single-cell data. Cell 2021;184:3573-3587.
7. Stoeckius M, Zheng S, Houck-Loomis B, et al. Cell Hashing with barcoded antibodies enables multiplexing and doublet detection for single cell genomics. Genome Biol. 2018;19: 224.
8. Luecken MD, Theis FJ. Current best practices in single-cell RNA-seq analysis: a tutorial. Mol Syst Biol. 2019;15:e8746.
9. Korsunsky I, Millard N, Fan J, et al. Fast, sensitive and accurate integration of single-cell data with Harmony. Nat Methods. 2019;16:1289-1296.
10. Andreatta M, Carmona SJ. UCell: Robust and scalable single-cell gene signature scoring. Comput Struct Biotechnol J. 2021;19:3796-3798.

11. Frankish A, Diekhans M, Ferreira AM, et al. GENCODE reference annotation for the human and mouse genomes. Nucleic Acids Res. 2019;47:D766-D773.
12. Ritchie ME, Phipson B, Wu D, et al. Limma powers differential expression analyses for RNA-sequencing and microarray studies. Nucleic Acids Res. 2015;43:e47.
13. Yaari G, Bolen CR, Thakar J, et al. Quantitative set analysis for gene expression: a method to quantify gene set differential expression including gene-gene correlations. Nucleic Acids Res. 2013;**41**:e170.
14. Hagan T, Gerritsen B, Tomalin LE, et al. Transcriptional atlas of the human immune response to 13 vaccines reveals a common predictor of vaccine-induced antibody responses. Nat Immunol. 2022;23:1788-1798.
15. Aran AP, Looney AP, Liu L, et al. Bhattacharya. Reference-based analysis of lung single-cell sequencing reveals a transitional profibrotic macrophage. Nat Immunol. 2019;20:163-172.
16. Monaco G, Lee V, Xu W, et al. RNA-Seq Signatures normalized by mRNA abundance allow absolute deconvolution of human immune cell types. Cell Rep. 2019;26:1627-1640.
17. Ellett F, Jalali F, Marand AL, et al. Microfluidic arenas for war games between neutrophils and microbes. Lab Chip. 2019;19:1205-1216.
18. Stewart A, Ng JC, Wallis G, et al. Single-Cell Transcriptomic Analyses Define Distinct Peripheral B Cell Subsets and Discrete Development Pathways. Front Immunol. 2021;12:602539.